Discovery of BMS-986365, a first-in-class dual androgen receptor ligand-directed degrader (AR LDD) and antagonist, for the treatment of advanced prostate cancer

Surendra Nayak[1], John D. Norris[2], Massimo Ammirante[1], Emily Rychak[1], Suzanne E. Wardell[2], Debbie Liao[1], Brandon Toyama[1], Raju Kandimalla[1], Andy Christoforou[1], Toshiya Tsuji[1], Ken Liu[1], Minerva Tran[1], Joseph Meiring[1], Samantha Reiss[1], Joseph R. Piccotti[1], Joshua M. Baughman[1], Celia Fontanillo[1], Marwa Khater[1], Deborah S. Mortensen[1], Brian Cathers[1], Neil Bence[1], Daniel W. Pierce[1], Veronique Plantevin-Krenitsky[1], Dana Rathkopf[3], Joshua D. Hansen[1], Lawrence G. Hamann[1], Rama Krishna Narla[1], Vivek K. Arora[1], Donald P. McDonnell[2], Mark Rolfe[1], and Shuichan Xu[1]

Author Affiliations: *[1]Bristol Myers Squibb, 10300 Campus Point Drive, Suite 100, San Diego, CA, USA 92121. [2]Duke University School of Medicine, 3 Genome Ct, Durham, NC, USA 27710. [3]Memorial Sloan Kettering Cancer Center, New York, NY, USA 10065.*

Present addresses for J.R. Piccotti, B. Cathers, D.W. Pierce, J.D. Hansen, and M. Rolfe may be available from corresponding author upon request

Running Title: BMS-986365, an AR degrader/antagonist for prostate cancer

Corresponding Author: Shuichan Xu, Oncogenesis Thematic Research Center, Bristol Myers Squibb, 10300 Campus Point Drive, Suite 100, San Diego, CA 92121. Phone: 858-926-6632; E-mail: shuichan.xu@BMS.com

Keywords: BMS-986365**,** Androgen receptor (AR), AR ligand-dependent degrader (AR LDD), degradation, prostate cancer, PROTAC, Targeted Protein Degradation

Disclosure of Potential Conflicts of Interest

Some of the studies described in this manuscript were supported by research grants from BMS to DPM and SEW. JDN and DPM have received consulting fees from BMS.

Authors' Disclosures

S. Nayak reports employment, patents, and stockholder with Bristol Myers Squibb. J. D. Norris consulting fees from Bristol Myers Squibb.

M. Ammirante, R. Kandimalla, A. Christoforou, K. Liu, S. Reiss, J. M. Baughman, D. S. Mortensen, B. Cathers, N. Bence, B. Toyama, R. K. Narla, and M. Rolfe report employment and stockholder with Bristol Myers Squibb.

E. Rychak, T. Tsuji, M. Tran, J. Meiring, and M. Khater report employment with Bristol Myers Squibb.

S. E. Wardell reports research funding to institution from Bristol Myers Squibb.

D. Liao, L. G. Hamann, and J. R. Piccotti reports no disclosures.

D. W. Pierce, C. Fontanillo, and V. K. Arora report employment, travel support, and stockholder with Bristol Myers Squibb.

V. Plantevin-Krenitsky reports employment, patents, and stockholder with Bristol Myers Squibb.

D. Rathkopf reports medical writing support from Bristol Myers Squibb; and participation on a data safety monitoring board or advisory board (no personal payment) from Bristol Myers Squibb, Johnson and Johnson, Genentech, Myovant, Promontory, Astra Zeneca, Bayer, Astellas, and Novartis.

J. D. Hansen reports employment and patents with Bristol Myers Squibb.

D. P. McDonnell reports research support and consulting fees from Bristol Myers Squibb.

S. Xu reports employment, travel support, patents, and stockholder with Bristol Myers Squibb.

ABSTRACT (254/250)

Purpose: BMS-986365, a heterobifunctional AR LDD, was designed as a potent cereblon-dependent degrader and competitive antagonist of AR to overcome resistance to ARPIs in metastatic prostate cancer (PC).

Experimental Design: *In vitro* impact of BMS-986365–induced AR degradation on AR activity and PC cell proliferation was evaluated. Intrinsic agonistic and antagonist activities of BMS-987365 were assessed. *In vivo* anti-tumor activity of BMS-986365 was compared with enzalutamide in multiple cell line- or patient-derived PC models.

Results: BMS-986365 is a potent, rapid, and selective degrader of AR wildtype and most of the clinically relevant mutants. Degradation of both wildtype and mutant AR is the key driver of BMS-986365 efficacy, with additional antagonism of residual AR activity enabled through occupancy of its ligand-binding domain. Compared with enzalutamide, BMS-986365 more efficiently inhibits AR target gene transcription and AR-dependent proliferation of PC cell lines. While enzalutamide increased AR protein in mCRPC models, BMS-986365 maintained low levels of AR protein despite increased AR transcript levels. *In vivo,* BMS-986365 demonstrated on-target activity, degrading AR, suppressing AR signaling, and inhibiting growth in validated cell line- and patient-derived xenograft models of castration-sensitive PC and advanced and/or therapy-resistant CRPC. Clinically, BMS-986365 reduced prostate-specific antigen in patients with mCRPC post ARPI, including patients with wildtype AR.

Conclusions: The preclinical observations, coupled with clinical data, strongly support the potential for BMS-986365 to overcome ARPI-resistant disease regardless of AR mutational status. These findings establish BMS-986365 as a first-in-class, dual AR degrader and competitive antagonist, likely to emerge as an important tool in the armamentarium to treat PC.

TRANSLATIONAL RELEVANCE

The androgen receptor (AR) is a key driver and therapeutic target for prostate cancer; however, resistance to AR pathway inhibition is an impediment to durable clinical responses. BMS-986365 is a heterobifunctional, ligand-directed degrader oral therapy designed to inhibit AR activity and overcome resistance via a first-in-class dual mechanism of AR degradation and antagonism.

INTRODUCTION

Metastatic prostate cancer (PC) is a disease of high morbidity, which, despite significant therapeutic advances, remains the second leading cause of cancer deaths in men (1). The majority of metastatic PCs are driven by the androgen receptor (AR) and regress following androgen deprivation therapy (ADT) via either surgical or medical castration. Inevitably, however, the disease progresses to metastatic castration-resistant prostate cancer (mCRPC), a stage for which approved endocrine therapies are ineffective. Decades ago, the hypothesis that incomplete AR inhibition achieved by ADT results in the emergence of mCRPC motivated the development of the first generation of direct AR antagonists (flutamide, bicalutamide, and nilutamide), all of which showed some clinical activity (2). However, the rapid emergence of resistance and the modest benefit afforded over castration alone have called into question the viability of AR as a therapeutic target in advanced disease (2). Some of the resistance to early AR inhibitors was attributable to mutations in the ligand-binding domain (LBD) of the receptor (AR^{L702H}, AR^{W742C}, AR^{H875Y}, and AR^{T878A}), which conferred ligand promiscuity, enabling its activation by nonandrogenic steroids (e.g., progesterone, glucocorticoids) and/or first-generation antiandrogens (3). Subsequently, it was discovered that AR gene amplification and/or overexpression emerges in the majority of tumors upon progression to mCRPC, and additional preclinical evidence indicates that AR overexpression is sufficient to drive mCRPC, reinvigorating interest in AR as a therapeutic target (4-6). Additional efforts to develop androgen receptor pathway inhibitors (ARPIs) were bolstered by the realization that the first-generation AR antagonists possess intrinsic partial agonism even towards wildtype (WT) AR and could exhibit growth-stimulatory activities in cells in which AR was overexpressed (5, 7). Second-generation AR antagonists, beginning with enzalutamide (ENZ), were developed using approaches that screened against intrinsic agonism of ligands in PC cells expressing high levels of AR (8). Clinical studies have now definitively established the superior

efficacy of second-generation AR antagonists (and highlighted the inverse correlation of agonist activity and magnitude of clinical benefit) and of abiraterone, an ARPI that diminishes adrenal androgen production via targeting CYP17A1 that also directly inhibits AR activity in patients with CRPC (9-13). Moreover, combining an ARPI with ADT as a primary intervention for patients with castration-sensitive prostate cancer (CSPC) induces more durable benefit and longer survival compared with castration alone (14-17).

Overcoming resistance to ARPIs has emerged as a major challenge in the treatment of patients with mCPRC. Correlative clinical evidence supports a continued role for AR, with disease progression typically occurring with a concurrent increase in prostate-specific antigen (PSA), a marker of AR activity. While effective, the currently available ARPIs appear to be limited in their ability to inhibit AR pathway activity, even when administered in early disease states (18). This may in large part be due to the disruption of a homeostatic negative feedback mechanism(s) that regulates AR expression and a concomitant increase in the expression of the receptor in cells in which androgen signaling is inhibited (19). Further, AR gene amplification and activating/altered specificity mutations, occurring at higher frequency in mCRPC in patients treated with ARPI versus treatment-naïve patients, also contribute to progression (20). In addition, upregulation of the expression of constitutively active AR splice variants (ARVs), which lack the C-terminal LBD, is often associated with AR gene amplification and overexpression and represents another mechanism implicated in the progression to CRPC (21).

Several new strategies have emerged to address the problem of continued AR activity in treatment-resistant PC. ODM-208 inhibits the enzyme CYP11A, which catalyzes the first step in steroid hormone biosynthesis and demonstrates activity in patients whose tumors express AR mutations that recognize nonandrogenic steroidal ligands as agonists (22). Some clinical activity has

been reported for EPI-7386, a drug that is purported to inhibit the activity of AR/ARVs by binding to the amino terminus of AR (23). A very promising new approach to target AR activity in advanced disease is through heterobifunctional small molecules that bind to the AR LBD, resulting in the recruitment of the receptor to the substrate recognition subunits of the E3 ubiquitin ligases cereblon (CRBN) or von Hippel Lindau for subsequent proteasomal degradation (24-27). Several heterobifunctional AR degraders, including ARV-110 (28), ARV-766 (29), HP518 (30), GDC-2992 (31), and AC0176 (32), have been described, some of which are being evaluated in clinical trials for therapeutic efficacy in patients with CRPC.

One of the challenges that has emerged in the development of heterobifunctional AR degraders is the identification of high-affinity AR binders that lack intrinsic agonism, an activity that would limit drug efficacy in the absence of complete receptor elimination. Addressing this issue, we report here the discovery of BMS-986365, a drug that was rationally designed to exhibit high receptor binding affinity while exhibiting low intrinsic agonist activity. This duality in its mechanism of action, degradation and competitive inhibition, enables BMS-986365 to achieve more potent and more profound inhibition of AR signaling compared with conventional antagonists. Importantly, this new drug inhibits tumor growth in clinically relevant cellular and animal models of mCRPC, including those resistant to ARPIs. These characteristics resulted in BMS-986365 being brought forward to clinical trials, where it has shown promise as a first-in-class representative of a new modality to treat patients with mCRPC.

MATERIALS AND METHODS

A high-level summary of the methods used is provided below. A more detailed description can be found in the Supplementary Methods.

Cell lines and compounds

The sources and status for AR and CRBN for PC lines used in this study are listed in Supplementary Table S1. VCaP (RRID:CVCL_2235) and LNCaP (RRID:CVCL_0395) were purchased from American Type Culture Collection (ATCC; Manassas, VA, USA) and were grown to 70% confluence before being passaged or incorporated into an experiment. Cell lines were used between passages 5 and 30. LNCaP cell lines were maintained in RPMI 1640 plus 10% fetal bovine serum (FBS) and VCaP cells were cultured in Dulbecco's Modified Eagle Medium (DMEM) plus 8% FBS in CellBIND flasks. All cell lines were routinely screened for mycoplasma contamination on a monthly basis during culture using the MycoAlert Mycoplasma Detection Kit (Lonza Cat# LT07-318) to ensure they remained free of contamination. The identity of the cell lines was authenticated by the vendor. EnzR VCaP is a human PC cell line resistant to ENZ, which was derived *in vivo* at Dr. Donald McDonnell's laboratory at Duke University from the VCaP parental cell line (ATCC). CWR22PC HR is a derivative of CWR22PC (RRID:CVCL_LI38), which was licensed from Dr. Marja T. Nevalainen's laboratory at the Medical College of Wisconsin, obtained *in vivo* by passaging the tumors three times in castrated male mice. HR-VCaP is a human castration-resistant PC cell line that was derived *in vivo* by serially passaging the tumors three times in castrated male mice. LNCaP cells expressing exogenous AR^{WT} (LNCaP-AR) or the F876L mutant (LNCaP-ARF876L) were generated at Dr. Donald McDonnell's laboratory at Duke University using retroviral transduction of receptor cDNA. LNCaP cells stably overexpressing mutants of AR driven by cytomegalovirus promoter were established and

used for the study. Lentiviral expression vector for AR^{WT}-Halo was purchased from Genecopoeia (Rockville, MD, USA, OmicsLink Expression Clone cat# EX-E2325-Lv211) and Halo-tag at C terminus was removed. DNA fragments carrying the corresponding AR mutations L702H, W742C, and H875Y were synthesized and cloned into pEZ-Lv211-AR vector using KpnI and NotI restriction enzyme sites. LNCaP cells were transfected with the DNA constructs using JetPrime transfection reagent (Polyplus Transfection, Illkirch, France) and selected with 1 μg/mL puromycin after 3 days of transfection. Stably transfected pool (L702H) or isolated single clones (W742C_clone #3.1 and H875Y_clone# 3.1.2) were used for the study. AR (WT, F877L, and L702H) was also overexpressed in PC3 cells (RRID:CVCL_0035) using the human ubiquitin C (UbC) promoter. Full-length WT, F877L, and L702H constructs of AR from pEZ-Lv211 vector were subcloned into pDONR 221 gateway vector (RRID: Addgene_118683) and recombined with the lentiviral vector pLoc_UBCP-3X-HA-pGK_Puro (RRID:Addgene_69053). Lentivirus was prepared for the various constructs using LentiX 293T cells (RRID:CVCL_4401), and PC3 cells were transduced and then selected with 1 μg/mL puromycin to establish stable pools that were used for various experiments. A new destination vector was constructed by inserting the coding sequence for the HiBiT tag (VSGWRLFKKIS) and a stop codon immediately following the 3× HA c-terminal HA tag in the pLoc_UBCP-3X-HA-pGK_Puro plasmid. The UbC promoter was then removed from this vector via digestion by ApaI and NotI, and the EF1a promoter inserted via in-fusion cloning according to the manufacturer's protocol. AR^{WT} cDNA was then recombined into this new Gateway lentivirus destination vector and used to make lentivirus. PC3 cells lacking endogenous AR expression were infected with the lentivirus and stable pools expressing HiBiT-tagged AR forms were used to isolate single clones using limited dilution followed by selection of the best clone based on moderate protein expression and HiBiT signal intensity. LNCaP cells with AR W74C knock-in (KI) mutant (LNCaP_AR.W742C_KI) was generated using CRISPR (HD Biosciences, San Diego, CA, USA) and

a single clone, B6, was used in this study. An LNCaP cell line with human CRBN knock-out (KO) was established using CRISPR/Cas9 technology (HD Biosciences) and a single clone, #C12, was used in all the experiments.

BMS-986365 was synthesized as shown in Supplemental Figure S1C. AR ligand-directed degrader (LDD) 1 and AR LDD2 were synthesized by methods analogous to BMS-986365 and as reported previously (33, 34).

Measurements of AR degradation by ELISA

The compounds were dissolved in dimethyl sulfoxide (DMSO) to prepare 10 mM stock solutions and then spotted in 96-well microtiter plates starting from 5 μM at 1:3 serial dilutions to generate a 10-point dose–response curve using an HP D300 Digital Dispenser. The cells were then added to the prespotted compounds in the 96-well plates at 50,000 for VCaP cells and 30,000 for LNCaP cells and LNCaP.CRBN.KO cells, and 20,000 LNCaP_AR^{WT}_OE per well in 200 μL growth medium. The cells were grown for 24 hours at 37°C with 5% CO_2 followed by aspiration of the media and cell lysis by incubating while shaking for 1 hour at 4°C with 100 μL 1X lysis buffer (component of Total AR ELISA kit) containing 1 mM phenylmethylsulfonyl fluoride. The cell lysates were either frozen at this stage or used for the AR ELISA assay with the Total Androgen Receptor ELISA Kit (Cell Signaling Technology, Danvers, MA, USA, cat# 12850). For kinetic studies to determine rate of AR degradation, cells were seeded (50,000 per well for VCaP and 30,000 per well for LNCaP) in a 96-well plate either in regular growth media or starved media (RPMI media without phenol red containing 5% charcoal-stripped fetal bovine serum [csFBS]). In order to starve the cells of androgen, cells were grown for 24 hours (VCaP) or 48 hours (LNCaP) and then treated with the compounds and R1881 at the indicated concentrations using an HP D300 Digital Dispenser (Hewlett Packard, Palo Alto, CA,

USA). The cells were then harvested at 15 and 30 minutes and 1, 2, 3, 4, 6, 16, and 24 hours and lysed; AR was quantitated by ELISA as described above.

Western blotting

For Western blot analysis, cells were grown in 6-well plates (500,000 for VCaP and 250,000 for LNCaP) in 2 mL regular growth medium or starvation medium and grown over night (48 hours for LNCaP cells to starve off the androgen). The cells were then treated with compound by replacing the media with media containing appropriate compound or R1881. Following incubation for the indicated duration, media was removed, cells were rinsed with Dulbecco's phosphate-buffered saline (DPBS), and 200 µL of 1X lysis buffer was added to each well. Cells were lysed by shaking for 1 hour at 4°C followed by transfer to 1.5 mL tubes using a cell scraper. Lysates were then vortexed and centrifuged at 15,000 g for 15 minutes at 4°C. For tumor samples, tissue samples (~50 mg) were homogenized in 1.5 mm zirconium beads (BeadBug) tubes with 600 µL Qiagen buffer RLT plus using a BeadBug homogenizer (3 cycles, speed 5, 30 seconds/cycle) and centrifuged for 15 minutes at 15,000 rpm at 4°C. The supernatant was taken and total protein estimated using a bicinchoninic acid (BCA) assay (Thermo Fisher Scientific Inc., Waltham, MA, USA, Cat. No. 23225); 10–30 µg of proteins were loaded for sodium dodecyl sulfate-polyacrylamide gel electrophoresis (SDS-PAGE) analysis and Western blot. Selectivity of degradation of AR over closely related steroid hormone receptors estrogen receptor (ER), progesterone receptor (PR), and glucocorticoid receptor (GR) was evaluated in T47D breast cancer cell line (RRID: CVCL_0553). T47D cells were grown in 10 cm dishes at 7 × 106 cells per dish in 10 mL RPMI containing 10% FBS and grown for 24 hours. The cells were then treated with BMS-986365 at 0.05, 0.5, and 5 µM concentrations (with or without CC-220 at 30 µM) and ENZ (5 µM), at 0.5 and 5 µM for 6 hours at 37°C. Following this, the incubation media was removed, cells were rinsed with DPBS, scraped, and centrifuged briefly to pellet down the cells.

Supernatant was removed and the cells lysed using 75 µL of 1X lysis buffer supplemented with protease and phosphatase inhibitors (MSD® Rockville, MD). Lysates were then vortexed and centrifuged at 15,000 g for 15 min at 4°C. The supernatant was taken, and total protein estimated using BCA assay. Lysates equivalent to 20 µg protein were loaded for SDS-PAGE analysis and Western blot using antibodies against human AR (Cell Signaling Technology Cat# 5153, RRID:AB_10691711), ER (Cell Signaling Technology Cat# 13258, RRID:AB2632959), GR (Cell Signaling Technology Cat# 12041, RRID:AB_2631286), and PR-A and PR-B (Cell Signaling Technology Cat# 3172, RRID:AB_331633).

Pulse SILAC liquid chromatography-mass spectrometry (LC-MS)

VCaP cells were plated at a density of 150,000 and 50,000 cells per well in the upper-half of eight 48-well and eight 96-well CellBIND plates respectively 1 day prior to compound treatment using DMEM-for stable isotope labeling with amino acids in cell culture (SILAC) media supplemented with 8% dialyzed FBS, normal L-lysine (100 mg/L), L-arginine (100 mg/L), and L-proline (230 mg/L). LNCaP cells were plated at a density of 60,000 and 20,000 cells per well in the bottom-halves of the above eight 48-well and eight 96-well CellBIND plates respectively 2 days prior to compound treatment using RPMI for SILAC media supplemented with 10% dialyzed FBS, normal L-lysine (100 mg/L), L-arginine (100 mg/L), and L-proline (230 mg/L). At day 0, seven plates of each set of 48-well and 96-well plates had the media switched to heavy isotope SILAC media, containing labeled L-lysine (2H4, 100 mg/L) and L-arginine (13C6, 100 mg/L), R1881 at 0.1 nM final concentration, and either DMSO, ENZ (1 µM), or BMS-986365 (100 nM and 1 µM), each condition in triplicate, and placed at 37°C. At 30 minutes and 1, 3, 6, 12, 24, and 48 hours, a 48-well and 96-well plate were taken and placed immediately on ice. The 48-well plate had media aspirated, was then washed twice with ice-cold PBS, and 60 µL of PreOmics iST lysis buffer (PreOmics GmbH, Planegg, Germany) was added

to each well. The plate was incubated on ice with intermittent shaking for 5 minutes and then frozen on dry ice and stored at −80°C until MS analysis. The 96-well plate was similarly aspirated and immediately frozen on dry ice and stored at −80°C for analysis by quantitative polymerase chain reaction (PCR). One plate each that did not have media changed (T=0) was taken down in a similar manner with the 1-hour time point.

Proteolytic digest and LC-MS-compatible peptide extraction was performed as described in the PreOmics' iST Sample Preparation Kit manufacturer's protocol, with a change of reducing the digestion buffer volume by half to account for the lower protein input. Extracted peptides were resuspended with 20 µL of PreOmics LC-Load buffer.

LC-MS data were acquired on a Thermo Orbitrap Fusion Lumos mass spectrometer (serial # FSN20472) coupled to a Thermo Dionex UltiMate 3000 nanoflow LC system (serial# 8145284). Approximately 1 µg peptide per sample was loaded onto an C18 trapping column (Thermo Scientific, Acclaim PepMap 100, 1.5 cm x 75 µm internal diameter, 3 µm particle size) at a flow-rate of 3.5 µL/min, followed by gradient elution from an EASY-Spray C18 liquid chromatography column (Thermo Scientific, 15 cm × 75 µm internal diameter, 1.8 µm particle size, 100 Å pore size) at a flow-rate of 0.30 µL/min. Peptides were separated with a linear gradient from 1.6% acetonitrile to 24% acetonitrile + 0.1% formic acid over 22 minutes, followed by a ramp to 72% acetonitrile over 1.5 minutes, at a constant flow-rate of 0.30 µL/min. The mass spectrometer was operated in positive ion-targeted tandem MS (MS/MS) acquisition mode. Each scan cycle was comprised of a precursor ion scan sampling mass-to-charge (*m/z*) range of 390–1500, followed by an MS/MS scans targeting precursor *m/z* 556.3272 and 559.3372, corresponding to AR peptide LLDSVQPIAR and heavy SILAC-labeled LLDSVQPIAR. MS and MS/MS scans were performed with Orbitrap mass resolution at *m/z*=200 of 120,000 and 60,000, respectively. Precursor ion scans were performed with automatic

gain control and maximum accumulation times of 4×10^6 and 100 ms, respectively. MS/MS scans were performed with a 1.5 Da precursor isolation window, normalized higher-energy collisional dissociation (HCD) collision energy set at 25, and automatic gain control of 5×10^5. In addition to the test samples, data were acquired for a serial dilution of a heavy isotope labeled AR LLDSVQPIAR peptide standard (New England Peptide Inc.), ranging from 2 to 250 fmol per sample, to establish assay limits of quantification.

LC-MS data files were processed in Skyline (version 22.2.0.255 [RRID: SCR_014080]). AR peptide identification was verified utilizing the AR peptide standard as a reference and confirmed by positive identification of the expected peptide sequence by the SEQUEST HT peptide-spectrum matching algorithm, as implemented in Thermo Proteome Discoverer (version 2.2 [RRID: SCR_014477]). Integrated peptide peak areas were normalized to sample total ion current and exported as tab-delimited tables. Turnover curve fitting for depletion turnover rates of both light and heavy isotope containing AR peptides were performed in GraphPad Prism (version 9 [RRID: SCR_002798]).

Evaluation of gene expression

A branched deoxyribonucleic acid (bDNA) assay was used to determine the inhibitory potency of each compound on R1881-stimulated AR target gene *FKBP5* expression. The housekeeping gene *RPL13A* was used as a normalization control.

VCaP cells in logarithmic phase growth were rinsed once with DPBS, dissociated with 0.25% trypsin, and collected in starvation medium (5% charcoal stripped FBS in 1X RPMI 1640 without phenol red). Cell counts were performed, and cells were resuspended to the appropriate concentrations in starvation medium. Cell suspension (200 µL per well) was plated in clear, flat-

bottom CellBIND 96-well plates and incubated at 37°C with 5% CO2 for at least 24 hours. Each test compound was added to the 24-hour-starved cell plates in a 10 point, 3-fold concentration series ranging from 0.0005 to 10 μM. CC-220 30 μM was dispensed into competition and control wells. R1881 was added for a final concentration of 0.3 nM in all wells, except for the starvation control DMSO wells. All wells were normalized with DMSO to a final concentration of 0.3% and incubated at 37°C and 5% CO_2 for 24 hours. To prepare cell lysates, the cell medium was carefully removed by aspiration and 200 μL of the bDNA diluted lysis working mixture were added to each well; the plates were covered and incubated at 50–55°C for 30 minutes to lyse the cells. Plates were then frozen at −80°C until time of use. The QuantiGene 2.0 Singleplex bDNA Assay was used to measure FKBP5 or the housekeeping gene RPL13A from cell lysates of cells treated with compounds following the manufacturer's instructions.

For data analysis, blank-subtracted target gene (*FKBP5*) relative light units (RLUs) were normalized to the blank-subtracted housekeeping gene (*RPL13A*) RLUs, yielding the target gene normalized ratio. Next, the normalized DMSO controls were subtracted from the target gene normalized ratios. To determine the target gene expression relative to the control for compounds tested as single agents in the presence of 0.3 nM R1881, the percent of control (POC) was calculated as follows:

POC = DMSO-subtracted target gene normalized ratio (compound wells)/DMSO-subtracted target gene normalized ratio of 0.3 nM R1881 control wells (no compound) × 100.

For compounds tested in competition with CC-220 in the presence of 0.3 nM R1881, the POC was calculated as follows:

POC = DMSO-subtracted target gene normalized ratio (compound wells)/DMSO-subtracted target gene normalized ratio of CC-220 with 0.3 nM R1881 control wells (no compound) × 100.

Excel/Xlfit4 was used to fit the data and generate IC_{50} values with the four-parameter logistic model or sigmoidal dose–response model (Fit Model 205), parameter restraints set to none. Means and standard deviations (SD) were calculated using Microsoft Excel. The mean POC and SD of the three independent runs were entered in an XY table format in GraphPad Prism. Graphs were plotted in GraphPad Prism with the dose–response: [inhibitor] versus response–variable slope (four parameters).

A Nanostring assay was developed to evaluate the expression of a panel of AR target genes in PC cells propagated *in vitro* and from xenograft tumor samples treated with indicated compounds. A custom NanoString nCounter Expression Array was designed and obtained from NanoString Technologies. VCaP and LNCaP cells were plated in a 96-well plate at 50,000 and 30,000 cells/well, respectively, in 100 µL/well phenol-red-free RPMI media containing 5% csFBS. After 24 hours of hormone starvation, the cells were treated with 0.1, 1, or 10 µM of DMSO, BMS-986365, or ENZ either with or without 0.3 nM R1881 using an HP D300 digital dispenser. BMS-986365 was added with or without CC-220 (30 µM). They were then incubated at 5% CO_2/37ºC for 6, 24, or 72 hours. After treatment with compound, the media was removed, and the cells were directly lysed by addition of Qiagen buffer RLT plus (15 µL/well). The cells were then homogenized by shaking for 1 minute, briefly centrifuged, and the lysates stored at −80ºC until use. For tumor samples: tissue samples (~30 mg) were homogenized in 1.5 mm zirconium beads (BeadBug) tubes with 600 µL Qiagen buffer RLT plus using a BeadBug homogenizer (3 cycles, speed 5, 30 seconds/cycle) and centrifuged for 15 minutes at 15,000 rpm at 4°C. RNA was isolated from supernatants using an RNeasy kit (Qiagen, Redwood City, CA, USA). All experiments were performed either in duplicate or triplicate, and in

accordance with the nCounter XT CodeSet Gene Expression assay (NanoString assay, NanoString Technologies, Seattle, WA, USA) manufacturer's manual. The NanoString data were analyzed using the R package "NanoStringNorm" The experiments were run in duplicate, and the data from the two runs were compiled and checked for control-gene performance (expression level and variation) and batch effect.

Total RNA (100 ng) was extracted from tumor tissues using RNeasy Kit (Qiagen) and was used as input for nCounter mRNA sample preparation reactions and these were performed according to the manufacturer's instructions (NanoString Technologies). The reactions were run using the nCounter Prep Station (NanoString Technologies). Data collection was carried out on the nCounter Digital Analyzer (NanoString Technologies) following the manufacturer's instructions to count individual fluorescent barcodes and quantify target RNA molecules present in each sample.

Proliferation assays

VCaP and LNCaP cells were re-suspended in phenol red-free RPMI 1640 plus 5% csFBS and passed through a 40-micron cell strainer to remove cell clumps. Cells were resuspended to 60,000 (VCaP) or 50,000 (LNCaP) cells per mL and dispensed by a Multidrop™ Combi Reagent Dispenser (ThermoFisher) into CellBIND 384-well plates at a final volume of 50 µL per well (3000 and 2500 cells per well for VCaP and LNCaP cells, respectively) and incubated in a 37°C incubator with 5% CO_2 for 24 hours for VCaP and 72 hours for LNCaP cells. The HP D300 Digital Dispenser (TECAN, Männedorf, Switzerland) was used to dispense compounds and R1881 at indicated final concentrations into black wall clear bottom 384-well plates to a final DMSO concentration of 0.1% in a maximum volume of 50 µL. A nine-point concentration/response assay starting at 10 µM with a 1:3 dilution was printed in duplicate. Plates were then incubated in a 37°C incubator with 5% CO_2 for

168 hours. For PC3 and 22Rv1 (RRID:CVCL_1045) cells, compounds were added to generate a 10-point dose response curve starting at 10 μM with 1:3 dilution in black wall clear bottom 384-well plates. PC3 and 22Rv1 cells were seeded at 2000 cells per well in 50 μL RPMI 1640 medium with 10% FBS and grown for 5 days. Assay plates and CellTiter-Glo (CTG) reagent were equilibrated at room temperature for 20 minutes. Using the Multidrop Combi Reagent Dispenser, 25 of CTG reagent or Caspase-Glo were added to each well, and then the plates were incubated at RT for 45 minutes. Luminescence was read using an EnVision plate reader (PerkinElmer, Waltham, MA, USA). For half-maximal growth inhibitory concentration (GI_{50}) values, relative luminescence readings were calculated by subtracting the background and normalizing to the DMSO control (100% of control). The GI_{50} was calculated using the following calculation, where T zero is the cell viability measurement without R1881 treatment:

1. G-PoC = ([compound treatment {%} − T zero {%}] / [100 − T zero {%}]) × 100

In vivo studies

All *in vivo* research protocols were approved by the BMS or Duke University or Champions Oncology Institutional Animal Care and Use Committee. Male 6- to 8-week-old intact or castrated NSG (NOD.Cg-*Prkdc*^{scid} *Il2rg*^{tm1Wjl}/SzJ [RRID:BCBC_46110]) or J/Nu mice were obtained from Jackson Laboratories (Bar Harbor, ME, USA). Mice were anesthetized with inhaled isoflurane and then inoculated with 5 × 10^6 VCaP or HR-VCaP cells or 2 × 10^6 patient-derived xenograft (PDX) cells (freshly isolated and dissociated from xenograft tumors) subcutaneously on the right flank with 0.2 mL of a single cell suspension containing 50% Matrigel using a sterile 1-mL syringe fitted with a 26-gauge needle.

Pharmacokinetic/pharmacodynamic studies

Groups of male intact NSG mice bearing VCaP tumors were dosed orally (PO) with vehicle (n = 8) or BMS-986365 (30 mg/kg) once daily (QD) for 3 consecutive days. The dosing started when the tumor volumes reached approximately 500 mm^3. To measure AR degradation in HR-VCaP model *in vivo*, castrated male NSG mice were inoculated with 5×10^6 HR-VCaP tumor cells into the right flank. Mice bearing castration-resistant VCaP tumors were randomized and dosed PO with vehicle or BMS-986365 (30 mg/kg) QD for 3 consecutive days. The dosing started when the tumor volumes reached approximately 500 mm^3. Blood and tumor samples were collected for compound measurement by LC/MS. Tumor samples were processed for evaluation of AR levels as pharmacodynamic markers using western blot technology.

To evaluate AR degradation in epididymis of higher preclinical species, male beagle dogs and sexually immature cynomolgus monkeys were dosed orally with BMS-986365 for 7 days QD at the indicated dose levels. At scheduled necropsy, tissues were obtained, fixed, and routinely processed for histopathology analysis. Sections of epididymis were examined for AR by immunohistochemistry (IHC). The AR IHC assay was performed using a Leica Bond automated slide stainer (Leica Microsystems Inc., Buffalo Grove, IL, USA) using the Bond Polymer Refine Detection Kit and accessory reagents. Formalin-fixed paraffin-embedded tissues were sectioned at 4 micron and deparaffinized on the Bond autostainer. Antigen retrieval was performed with Epitope Retrieval 1 (ER1, pH 6.0) for 20 minutes at 100 °C. The slides were blocked for endogenous peroxidase activity with Peroxide Block for 5 minutes at RT. Sections were then incubated with the rabbit monoclonal antibody anti-AR (Abcam, Cambridge, United Kingdom, Catalog No. Ab133273) at 1:800 dilution for 15 minutes at RT, followed by horseradish peroxidase-labeled Polymer at the instrument's default condition. Antigen–antibody complex was then visualized with hydrogen peroxide substrate and diaminobenzidine tetrahydrochloride chromogen. After IHC staining, slides were dehydrated by passage through graded alcohols to xylene then coverslipped.

Efficacy studies

For efficacy studies in intact mice, groups of male J/nu mice bearing indicated xenograft tumors (n = 4–7/group) were dosed PO with vehicle, BMS-986365 or ENZ QD for various consecutive days at the indicated doses. The dosing started when the tumor volumes reached approximately 150 mm^3. Thereafter, tumors were measured three times weekly for the duration of the study. The long and short axes of each tumor were measured in millimeters using a digital caliper. The tumor volumes were calculated using the formula:

$W^2 \times L/2$ (long [L] and short [W] axes of tumors).

For efficacy study in HR-VCaP model, castrated male NSG mice were inoculated with 5×10^6 HR-VCaP tumor cells into the right flank. Mice were randomized into treatment groups (n = 10/group) at the time of treatment initiation. Groups of mice bearing VCaP tumors (n = 10/group) were dosed PO with vehicle, BMS-986365 (30 mg/kg) or ENZ (50 mg/kg) QD for 45 consecutive days. The dosing started when the tumor volumes reached approximately 200 mm^3.

Patient Case Study

The first-in-human study protocol was approved by either the institutional review board or independent ethics committee at the participating institutions. The study was conducted in accordance with the Declaration of Helsinki, the International Conference on Harmonization Good Clinical Practice guidelines, and applicable local and regulatory requirements and laws. Informed consent was documented prior to the patient's entry into the study. Details on patient dosing, assessments, guidelines, and informed consent are available in the publication of the first-in-human trial of BMS-986365 (35).

Data Availability Statement

RNA-seq data is available at the Gene Expression Omnibus (GEO) (RRID:SCR_005012) (GSE298071). Bristol Myers Squibb's policy on data sharing and the data request form may be found at https://www.bms.com/researchers-and-partners/independent-research/data-sharing-request-process.html.

RESULTS

Discovery of BMS-986365, an AR degrader that balances degradation potency and intrinsic agonism

AR is unique among the nuclear receptors as high-affinity binding of an agonist requires a specific interaction between the amino terminus and the carboxyl terminus of the protein. High-affinity agonist binding results in the formation of a coactivator binding surface that tracks with agonism (36). This has limited the development of potent AR antagonists since the affinity of molecules that bind to the classic LBD of the receptor appears to be inextricably linked to increased agonist activity (36-38). Thus, to develop a CRBN-based heterobifunctional AR degrader with low intrinsic agonistic activity, we developed a strategy that balanced degradation potency and efficiency, inherent agonist/antagonist properties, and the drug-like properties of molecules (Supplementary Fig. S1A). Specifically, we took an empirical approach by screening compounds from multiple chemical series using cell-based assays as illustrated in Supplementary Fig. S1A. The primary assay was an AR ELISA performed using VCaP cells to determine degradation potency. Active compounds were then tested in secondary assays designed to determine the relative agonist and antagonist biocharacter of newly identified AR modulators. The inherent agonist activity of the AR LDDs was evaluated by assessing their ability to induce AR target gene expression (i.e., *FKPB5*) or cell proliferation in the presence or absence of CC-220, a high-affinity competitive CRBN binder that blocks CRBN-mediated AR degradation (39). In a structure-activity relationship (SAR) study of a large number of compounds,

we observed, as expected, that increased degradation potency was associated with an increase in intrinsic agonism (Supplementary Fig. S1B). This relationship is exemplified by the results of studies evaluating two compounds emerging from our drug discovery program, AR LDD1 and AR LDD2 (Fig. 1A, Supplementary Fig. S1C). AR LDD1 is a very potent AR degrader (half-maximal degradation concentration [DC_{50}]: 1 nM) and displayed potent degradation-driven antiproliferative activity (GI_{50}: 1 nM; Supplementary Table S2; Fig. 1B). However, when degradation was blocked by coadministration of CC-220, a high-affinity competitive CRBN binder, high intrinsic agonism was observed as measured by both *FKBP5* gene expression and cell proliferation (Supplementary Table S2; Fig. 1C) and by its limited intrinsic antagonistic activity in assays that assess androgen-dependent proliferation of PC cells (GI_{50}: ~3.0 μM; Fig. 1B; Supplementary Table S2). AR LDD2 is a compound with significantly reduced intrinsic agonism but also with diminished AR degradation potency compared with AR LDD1 (DC_{50}: 83 nM; Fig. 1C; Supplementary Table S2). As a result, in the presence of CC-220, AR LDD2 has slightly better intrinsic antagonist activity (GI_{50}: ~1.6 μM [AR LDD2] vs. ~3.0 μM [AR LDD1]), but its degradation-driven antiproliferative activity in the absence of CC-220 (GI_{50}: 84 nM for AR LDD2 vs. 1 nM for AR LDD1) is severely attenuated. Leveraging insights such as these led to the identification of BMS-986365, which was selected for development as it achieved a balance of improved AR degradation potency compared with AR LDD2 and exhibited significantly lower intrinsic agonism than AR LDD1. Importantly, the intrinsic antagonism manifested by BMS-986365 is similar to that of ENZ (GI_{50}: 753 nM vs. 977 nM; Supplementary Table S2), and it is a more potent antagonist than either AR LDD1 or AR LDD2 in VCaP (AR^{WT} amplified) cells (Supplementary Table S2; Fig. 1B).

BMS-986365 binds with high affinity to AR and induces its proteasome-dependent degradation

BMS-986365 is an AR LDD that contains a receptor-binding moiety connected via a short linker to a CRBN-binding moiety (Fig. 2A and Supplementary Fig. S1C). This drug binds AR with an affinity similar to that of testosterone (T) and ~10-fold higher than that of ENZ (Supplementary Table S3; Supplementary Fig. S2A). The ability of BMS-986365 to facilitate CRBN- and proteasome-dependent AR degradation was first evaluated in VCaP cells. Cells were treated for 6 hours with BMS-986365 (0.1 μM or 1.0 μM) alone or in combination with a proteasome inhibitor (MG132), a neddylation inhibitor that inactivates cullin–RING E3 ligases (MLN4924) (40), or the high-affinity competitive CRBN binder, CC-220 (Fig. 2B). Western immunoblot analysis indicated strong degradation of AR with BMS-986365 treatment alone, which was not seen in cells co-treated with MG132, MLN4924, or CC-220. Similarly, BMS-986365 treatment resulted in CRBN-dependent degradation of an AR^{WT}-HiBiT tag fusion protein expressed in PC3 cells from a heterologous promoter (Supplementary Fig. S2B). Finally, we demonstrated that inhibition of the binding of BMS-986365 to AR using high concentrations of the synthetic androgen R1881 as a competitor prevented receptor AR degradation (Supplementary Fig. S2C). These results confirm the on-target activity of BMS-986365 and demonstrate that BMS-986365 is active in the presence of androgens. Collectively, these data indicate that BMS-986365 interacts with AR with high affinity and selectively directs its CRBN-dependent proteasomal degradation.

BMS-986365 displayed rapid AR degradation kinetics that were manifested in a concentration-dependent manner *in vitro* (Fig. 2C and D). Both AR^{WT} and AR^{T878A} were rapidly degraded by BMS-986365, with maximal degradation observed within 6 hours at concentrations of BMS-986365 ≥50 nM and 500 nM in VCaP and LNCaP cell lines, respectively (Fig. 2C; Supplementary Fig. S2D). The rate of AR degradation by BMS-986365, expressed as $t_{1/2}$, was concentration-dependent in both cell lines (Supplementary Table S4). Specifically, the $t_{1/2}$ for AR degradation for BMS-986365 at 500 nM was

~0.6 hours and ~1.3 hours, respectively, for VCaP and LNCaP cells. In VCaP cells, BMS-986365, at a concentration as low as 50 nM, reduced AR to 50% of the DMSO control within 2 hours, with maximal AR reduction achieved by 6 hours and sustained through 24 hours (Fig. 2C). In LNCaP cells, a higher concentration of BMS-986365 (500 nM) was needed to achieve a similar level of degradation, reflecting a difference in degradation potency in these two cell lines (DC_{50}: 7 nM in VCaP vs. 29 nM in LNCaP; Supplementary Table S5). This is likely due to lower CRBN and AR expression in LNCaP cells when compared to VCaP cells (Supplementary Fig. S2E). When AR was exogenously expressed in PC3 cells, BMS-986365 showed similar degradation potency for AR^{WT} and AR^{T878A} (Supplementary Table S6). AR degradation induced by 50 nM or 500 nM of BMS-986365 led to complete inhibition of R1881-stimulated expression of FKBP5 and PSA proteins in VCaP cells as measured by western immunoblot (Fig. 2D). To measure the absolute rates of AR degradation induced by BMS-986365, we performed pulse stable isotope labeling of amino acids in cell culture (SILAC), switching cells to media containing heavy isotopes of lysine and arginine coincident with compound treatment. Subsequently, light (old) peptide isotopes and heavy (new) peptide isotopes were identified and quantified by mass spectrometry. Using this approach to assess turnover in VCaP and LNCaP cells revealed that the half-life of AR was 4.3 hours and 3.9 hours in vehicle-treated cells, respectively. (Fig. 2E and 2F; Supplementary Table S7). In contrast, treatment with 100 nM BMS-986365 decreased AR half-life to 0.55 hours (VCaP cells) and 0.95 hours (LNCaP cells), reaching the limit of quantitation by 3 hours and 1 hour, respectively (Fig. 2E and 2F). ENZ treatment had no impact on AR turnover rates in either cell line. Thus, using multiple approaches, we confirmed that BMS-986365 induces rapid and quantitative degradation of AR.

To determine the target selectivity of BMS-986365, we performed global proteomics in LNCaP cells treated with 1 μM BMS-986365 for 6 hours and assessed changes in proteins compared with a

DMSO control (Supplementary Fig. S2F). Analysis of these data indicated, as expected, that 1 μM BMS-986365 degraded AR protein to 15% of that in vehicle (DMSO)-treated cells (adjusted $P = 2.3 \times 10^{-6}$) with no other protein changing more than two-fold (adjusted $P \leq 0.01$), out of 8342 proteins quantified. Known CRBN neosubstrates, including ZFP91, GSPT1, and CSNK1A1, were detected but not significantly degraded by BMS-986365. In addition, no degradation of the close AR family members ER, PR, or GR was observed (Supplementary Fig. S2F).

The ability of BMS-986365 to induce the degradation of AR in cells with AR overexpression or in cells expressing clinically relevant AR mutants was also examined. The degradation potency of BMS-986365, defined as the concentration required to achieve 50% degradation of AR (DC_{50}) relative to AR levels in DMSO-treated cells, ranged from 6 nM to 47 nM for amplified AR^{WT} and select AR mutants (e.g., AR^{T878A}, AR^{H875Y}, AR^{W742C}, and AR^{F877L}; Supplementary Table S5). The degradation efficiency (Y_{min}), which measures the extent of BMS-986365-induced degradation by comparing the residual AR level upon BMS-986365 treatment with that in DMSO-treated control cells, ranged from 7% to 17% for AR^{WT} and mutant forms (Supplementary Table S5). BMS-986365 did not efficiently degrade AR^{L702H}, exhibiting a DC_{50} of 1.5 μM and a Y_{min} of 41%. Interestingly, this drug is a potent degrader of the $AR^{T878A/H875Y}$ and $AR^{T878A/L702H}$ double mutants with DC_{50} values of 19 nM and 59 nM, respectively. BMS-986365 does not degrade ARV7 (Supplementary Table S5). Therefore, BMS-986365 is a potent, efficient, and selective AR degrader of AR^{WT} and most of the clinically relevant AR mutants.

BMS-986365 is both a competitive antagonist and a degrader of AR

The functional consequence of BMS-986365-induced AR degradation was evaluated in multiple assays in PC cell lines that model CRPC secondary to AR overexpression or to the

expression of clinically relevant AR mutations. To demonstrate on-target anti-proliferative activity, BMS-986365 was evaluated in AR+ and AR-dependent VCaP and LNCaP cells, AR+ and ARV7-dependent 22Rv1 cells (41), and AR negative PC3 cells. BMS-986365 potently inhibited androgen-stimulated proliferation of VCaP and LNCaP cells but showed little anti-proliferative effect in 22Rv1 or PC3 cells (Fig. 3A and Supplementary Table S8). We then evaluated the ability of BMS-986365 to inhibit R1881/AR-dependent expression of *FKBP5* mRNA in both VCaP and LNCaP cells *in vitro* using a quantitative branched DNA assay (Fig. 3B; Supplementary Fig. S3A). BMS-986365 exerted a potent inhibitory effect on androgen-upregulated *FKBP5* expression, with IC_{50} values of 1 nM and 4 nM for VCaP and LNCaP, respectively, which were 1–2 orders of magnitude more potent than those of ENZ (Supplementary Table S9). The potent inhibition of AR-dependent transcription by BMS-986365 correlated with its ability to inhibit AR-dependent proliferation (Fig. 3C; Supplementary Fig. S3B). BMS-986365 inhibited R1881-stimulated proliferation of VCaP and LNCaP cells with GI_{50} values of 11 nM and 4 nM, respectively, which were ~50–100-fold more potent than those of ENZ (Supplementary Table S8).

The contribution of AR degradation to the antagonist efficacy of BMS-986365 was evaluated by assessing the inhibition of AR target gene expression and cell proliferation in the presence of CC-220. When BMS-986365-mediated AR degradation was blocked by CC-220, the AR antagonist activity of BMS-986365 was substantially attenuated, as measured by *FKBP5* expression (34- and 22-fold increase of IC_{50} values for VCaP and LNCaP, respectively) or proliferation (66- and 169-fold increase of GI_{50} values, for VCaP and LNCaP, respectively; Fig. 3B and 3C; Supplementary Table S8 and S9), suggesting that AR degradation is the primary mechanism by which this drug inhibits androgen action. Importantly, however, even when AR degradation was blocked, BMS-986365 displayed substantial intrinsic antagonist activity, reflecting the inherent capability of the compound to

function also as a classic competitive antagonist, exhibiting a potency similar to that of ENZ for AR^{WT} and slightly less potency than that of ENZ for the AR^{T878A} mutant form (Fig. 3B and 3C; Supplementary Fig. S3A and S3B; Supplementary Table S8 and S9). Consistently, CC1082007, the AR-binding moiety of BMS-986365 devoid of the CRBN-binding component, showed antagonist activity with potency comparable or better than ENZ (Supplementary Fig. S3C and Supplementary Table S9).

Having established its unique dual mechanism of action, we next evaluated the impact of BMS-986365 on a broad panel of AR-regulated genes, using a NanoString-based assay we developed, which allowed an assessment of 114 AR-regulated and 19 housekeeping genes in both VCaP and LNCaP cells. BMS-986365 substantially reversed R1881 (0.3 nM) mediated AR-dependent transcription in both cell lines, whereas ENZ only modestly reversed R1881-mediated gene expression changes under the same conditions (Fig. 3D; Supplementary Fig. S3D; the gene list and normalized data are included in Supplementary Table S10). Furthermore, the ability of BMS-986365 to inhibit R1881-dependent gene expression occurred much more rapidly (i.e., 6 hours for VCaP) than with ENZ, which only accomplished inhibition at higher concentrations and with a longer duration of treatment (24 hours to 72 hours post-treatment) in the same models. When AR degradation was blocked by CC-220, BMS-986365 still displayed AR antagonist activity, as measured by its ability to inhibit the expression of multiple AR target genes using a NanoString assay (Fig. 3E; the gene list and normalized data are included in Supplementary Table S10). These data indicate that in relevant models of PC, BMS-986365 displays a dual mechanism of action, functioning both as a classic AR antagonist and as a receptor degrader.

To evaluate the impact of its dual mechanism of action (degradation and competitive antagonism), we compared the activity of BMS-986365 with ARV-110 in VCaP cells. Both compounds

showed similar AR degradation potency and depth, but ARV-110 displayed higher intrinsic agonism for AR^{WT} when degradation was blocked by CC-220 (Supplementary Fig. S3E and Supplementary Table S11). Consistently, ARV-110 showed less intrinsic antagonist activity (GI_{50} >10 μM) than BMS-986365 when AR degradation was blocked. Importantly, even without interfering with AR degradation, it was observed that ARV-110 displayed almost 10-fold less potent anti-proliferative activity than BMS-986365 (GI_{50} 95 vs. 11 nM), despite their similar degradation profiles, suggesting that both AR degradation and intrinsic antagonism contribute to the potent and efficacious anti-proliferative activity of BMS-986365. To prove that AR degraders bind to residual AR, we used a lower concentration of CC-220 (0.5 μM) to block AR degradation to ~50% of AR relative to DMSO-treated VCaP cells and tested if an AR degrader like AR LDD1, which has high intrinsic agonist activity, would stimulate VCaP cell proliferation under these conditions (Supplementary Fig. S3F). Both BMS-986365 and AR LDD1 at concentrations of 12 and 37 nM achieved ~50% AR degradation in the presence of 0.5 μM CC-220. Under these conditions, AR LDD1, but not BMS-986365, stimulated VCaP cell proliferation to ~200% of the DMSO-treated control, indicating that AR degraders bind to residual AR and can stimulate AR activity if they have high intrinsic agonist potential.

Studies to evaluate the ability of BMS-986365 to inhibit PC proliferation in different models of CRPC were undertaken. It was determined that BMS-986365 inhibited R1881-stimulated cell proliferation of LNCaP cells overexpressing exogenous AR^{WT} or one of several AR mutant forms (AR^{F877L}, AR^{H875Y}, or AR^{W742C}) with GI_{50} values ranging from 3 nM to 36 nM (Supplementary Table S8). The GI_{50} values of ENZ ranged from 0.12 μM to 1.35 μM in the same cell lines, approximately 10- to 120-fold less potent than BMS-986365. Consistent with our observation that BMS-986365 is a less potent degrader of the AR^{L702H} mutant, it was also less potent in assays that evaluated the proliferation of cells expressing this mutant (GI_{50} value of 0.24 μM), albeit ~10-fold more potently than

ENZ. Reflecting the ability of BMS-986365 to function as both a competitive inhibitor and a degrader of AR, we determined that treatment with CC-220 attenuated but did not abolish the antiproliferative activity of the drug in cells overexpressing AR^{WT} or those expressing clinically relevant mutants, including L702H. BMS-986365 displays intrinsic antagonist activity (GI_{50} value of ~0.93 μM) on this mutant, which is further enhanced by modest CRBN-mediated degradation. BMS-986365 does not inhibit the proliferation of ARV7-dependent 22RV1 (41) or AR-negative PC3 cell proliferation (Fig. 3A; Supplementary Table S8). Collectively, these data suggest that removal of AR via BMS-986365-mediated degradation is more effective at antagonizing R1881-induced AR function than is ENZ, a reversible AR antagonist, in both AR^{WT}-amplified and AR-mutant models. Additionally, the data suggest that AR degradation is the key driver of BMS-986365 AR inhibitory potency, which is reinforced by its considerable intrinsic antagonist activity.

BMS-986365 degrades AR *in vivo* and demonstrates antitumor activity in multiple models of CSPC and mCRPC that exhibit resistance to contemporary ARPIs

In vivo, BMS-986365 demonstrated an acceptable pharmacokinetic profile with good oral bioavailability observed in several preclinical animal models (Supplemental Fig. S4A). Following a single intravenous (IV) administration of BMS-986365 to CD1 mice at 2 mg/kg, the plasma clearance of BMS-986365 was 20.7 mL/min/kg. The observed volume of distribution was 3.1 L/kg resulting in a half-life of 1.7 hours (Supplementary Table S12). Oral administration of BMS-986365 resulted in a mean peak plasma concentration (C_{max}) of 0.275 μM at a mean time to reach (T_{max}) of 4.5 hours. The systemic bioavailability (%F) of BMS-986365 in CD1 mice at this dose was 40%. The product of the fraction absorbed, and the fraction of the compound escaping the gut (fa x fg) was estimated to be 0.6 (Supplementary Table S13).

The *in vivo* degradation efficacy of BMS-986365 was assessed in VCaP tumors propagated in intact NSG™ male mice dosed orally with vehicle or BMS-986365 (30 mg/kg) once daily for 3 consecutive days. Evaluation of plasma and tumor samples indicated good compound exposure in both the circulation and within tumors at 2 hours, 6 hours, and 24 hours post-last dose (Fig. 4A). Intratumoral levels of AR and the expression of AR target genes were measured in tumors harvested at the indicated time points. BMS-986365 reduced AR to 91% and 83% of control levels at 6 hours and 24 hours, respectively, post-last dose (Fig. 4A). Similar AR degradation was observed in VCaP tumors grown in castrated mice (Supplementary Fig. S4B). In a previous study, we defined a list of 152 genes involved in cell-cycle regulation/cell proliferation, which were regulated by androgens in cellular models of PC (42). Expression of these genes was significantly and substantially suppressed by BMS-986365 at both 6 hours and 24 hours post-treatment in a VCaP xenograft study performed in intact mice (Fig. 4B), confirming that BMS-986365 suppressed AR signaling. Importantly, dose-dependent degradation of AR in the epididymis of both dog and sexually immature monkey (Fig. 4C) was also observed, suggesting that BMS-986365 can induce deep AR degradation *in vivo* across different mammalian species.

When dosed at 30 mg/kg PO, BMS-986365 exhibited significant antitumor activity in a VCaP xenograft model exhibiting 81% and 76% tumor volume reduction (TVR) in intact (Fig. 4D) or castrated mice (Supplementary Fig. S4B), respectively. As a comparator, ENZ (30 mg/kg) showed only moderate antitumor activity (51% TVR) in VCaP tumors propagated in intact mice (Fig. 4D). Importantly, BMS-986365 also showed dose-dependent antitumor activities in a VCaP model of acquired resistance to ENZ (ENZR; Fig. 4E).

To support and direct the clinical development of BMS-986365, the antitumor activity of BMS-986365 was also evaluated in PDXs that model different PC disease states. BMS-986365 effectively

blocked tumor growth in three PDX models of CSPC (Supplementary Fig. S4C; Supplementary Table S14). ENZ showed similar antitumor activity to that of BMS-986365 in the OMP-PR3 model but was much less efficacious in two other models of CSPC (OMP-PR22 and OMP-PR23). As expected, neither BMS-986365 nor ENZ were active in the AR-negative OMP-PR16 model. In addition, BMS-986365 degraded tumor AR and demonstrated better antitumor activity than ENZ in the PCSD1 PDX model isolated from a patient with ARPI-naive CRPC who had progressed on ADT (Supplementary Fig. S4D) (43). Nanostring analysis using AR and neuroendocrine gene signatures confirms that the AR+ PC models cluster together while two AR-negative models (PC3 and OMP_PR16) form a separate cluster (Supplementary Fig. S4E). These data highlight the likely utility of AR degradation as a therapeutic strategy in patients with either CSPC or CRPC with *de novo* or acquired resistance to standard-of-care endocrine therapies.

BMS-986365 overcomes resistance to ARPIs that results from an adaptive increase in AR expression in tumors

Consistent with previous results (19), we observed that R1881 decreased both AR mRNA and protein levels in VCaP cells (Supplementary Fig. S5A). Further, it was determined in this cell line that both ENZ and BMS-986365 reversed this suppressive activity on *AR* expression, leading to an induction of AR mRNA expression (Supplementary Fig. S5B; Supplementary Table S15). The ENZ-induced increase in AR mRNA subsequently resulted in a commensurate increase in AR protein. Conversely, treatment with BMS-986365 did not result in AR protein accumulation, despite increased AR mRNA levels. In LNCaP and MDA-PCa-2b cells, R1881 had little effect on AR mRNA levels but did result in the upregulation of AR protein levels. Regardless, in LNCaP cells, BMS-986365, but not ENZ, decreased AR protein levels. SILAC experiments in these cells confirmed that new AR synthesis plateaued at ~91% and 134% for the DMSO and ENZ groups in VCaP cells, but 98% and

86%, respectively, in LNCaP cells (Supplementary Fig. S5C and S5D; Supplementary Table S16). These data demonstrate that AR upregulation in VCaP, but not LNCaP cells, by ENZ was likely due to increased AR synthesis via transcriptional upregulation. In both cell lines, BMS-986365 was able to rapidly and efficiently degrade the newly synthesized AR to a level below that of detection at both 0.1 µM and 1 µM. Collectively, the data suggest that although some PC cells/tumors can upregulate AR mRNA/protein expression in response to AR inhibition, this activity, which is likely a key driver of resistance to ARPIs, can be overcome by BMS-986365-dependent receptor degradation.

We next explored the impact of AR upregulation, frequently seen in patients with CRPC, on the response to BMS-986365 or ENZ in disease-relevant tumor models (Fig. 5; Supplementary Table S17). We employed two PDX tumor models, CTG-2441 and CTG-2440, which were derived from bone metastases of the same patient following progression on ADT or ADT plus abiraterone treatments, respectively (Fig. 5A, top). We confirmed that these models express AR^{WT} without gene amplification (Supplementary Table S17). RNA-sequencing (RNA-seq) analysis of the tumor samples revealed that AR mRNA levels were higher in the tumor samples from CTG-2440 than those from CTG-2441 (Fig. 5A, bottom left). Interestingly, AR activity, inferred from AR target gene expression, was similar in the two models (Fig. 5A, bottom right). Pharmacodynamic studies were performed in mice harboring CTG-2441 or CTG-2440 xenografts treated with BMS-986365 or ENZ once daily for 7 consecutive days, and tumor samples were collected for western immunoblot and RNA-seq analyses after the final dose. In the CTG-2441 PDX model, treatment with either compound led to an increase in AR mRNA levels (Fig. 5B, top middle; Supplementary Table S18); however, BMS-986365, but not ENZ, reduced AR protein levels (Fig. 5B, top left). Both compounds significantly and substantially inhibited AR activity (Fig. 5B, top right; Supplementary Table S18) and inhibited tumor growth (Fig. 5B, bottom). In the CTG-2440 PDX model (Fig. 5C, top panel; Supplementary Table S18), 7 days of

treatment with either compound resulted in an increase in tumor AR mRNA levels. BMS-986365, but not ENZ, reduced AR protein levels in tumor samples after 7 days of compound treatment. Both compounds inhibited AR activity as measured by target gene expression, with a trend towards deeper inhibition of AR signaling by BMS-986365. Importantly, BMS-986365 demonstrated superior antitumor activity compared with ENZ in this model (Fig. 5C, bottom right). Interestingly, in tumor samples collected at the end of the efficacy study, it was observed that AR protein levels were substantially increased in the ENZ-treated samples, whereas BMS-986365 maintained suppression of AR protein at levels lower than those in vehicle-treated tumors (Fig. 5C, bottom left). These data highlight the favorable activity of BMS-986365 in two different models of CRPC and indicate that the upregulated AR expression observed in some models/patients in response to ARPIs is likely to impact the therapeutic efficacy of ARPIs, which can be overcome by BMS-986365.

PSA and radiographic response to BMS-986365 in a patient with mCRPC who progressed on ENZ

Consistent with the preclinical findings described above, BMS-986365 has shown preliminary efficacy in patients with ARPI-resistant mCRPC (35). CC-94676-PCA-001 (NCT04428788) is a phase I, multi-center, open-label, dose-finding study in patients with mCRPC that previously progressed on an ARPI. Primary objectives were safety and tolerability, maximum tolerated dose, and/or recommended phase II dose. Secondary objectives were preliminary efficacy measured by PSA, objective soft tissue response, and pharmacokinetics.

The patient presented here is a 69-year-old Caucasian male with an initial diagnosis of localized Gleason 7 adenocarcinoma of the prostate treated initially by prostatectomy, who later received salvage radiation therapy with ADT. Previous systemic treatments for his recurrent/metastatic disease included leuprolide, bicalutamide, ENZ, talazoparib, and avelumab.

Progression on prior ENZ was demonstrated by both rising PSA levels and imaging. The patient was assigned to receive treatment with BMS-986365 at a dose level of 400 mg twice daily. At the start of treatment, PSA was reported as 59.97 µg/L. Baseline CT scan identified an enlarged para-aortic lymph node that met RECIST criteria for a target lesion, in addition to two nontarget lymph-node lesions. Baseline genomic testing by circulating tumor DNA analysis identified AR amplification and a *BRCA2* mutation. No AR LBD mutations were detected.

By cycle 1 day 15, the patient's PSA had declined by more than 90% (PSA90) to 4.95 µg/L (Fig. 6A). PSA was measured on the first day of each 28-day cycle and achieved a nadir of 1.49 µg/L at cycle 7. PSA90 was sustained until cycle 12. The rapid and deep decline in PSA was accompanied by radiographically evident antitumor activity, with the first on-treatment radiographic assessment at 8 weeks demonstrating a complete response in the target lesion and an overall partial response based on RECIST criteria (Fig. 6B). The radiographic partial response was maintained for approximately 65 weeks, at which time there was progression in the target lesion and the participant discontinued treatment. Adverse events suspected to be related to study treatment were limited to grade 1 sinus bradycardia and grade 1 QTc prolongation. Overall, these results illustrate the ability of BMS-986365 to induce clinically meaningful benefit in patients with ARPI-resistant mCPRC with minimal toxicity.

DISCUSSION

Drugs that inhibit AR signaling remain frontline treatments for patients with PC at all stages (44). While contemporary AR antagonists and inhibitors of androgen biosynthesis have been shown to be effective, *de novo* and acquired resistances remain significant impediments to durable clinical responses (45). Genomic analysis of tumor biopsies suggests that the majority of tumors from patients with mCRPC express AR^{WT} with or without gene amplification, with AR LBD mutations occurring in approximately 15%–30% of the mCRPC patient population (4). The frequency of AR gene alterations modestly increases in ARPI-exposed vs. naïve mCRPC, supporting continued selective pressure for strategies to upregulate AR activity (20, 46, 47). We hypothesize that even in patients whose tumors are resistant to drugs such as ENZ and abiraterone, AR remains engaged in the regulation of processes of pathological importance and that the inability of current inhibitors to fully block AR activity in tumors in which it is overexpressed or mutated is a significant liability of existing medicines. This puts in context our discovery of BMS-986365, a first-in-class dual AR degrader and inhibitor, as a new approach to treat patients whose tumors are resistant to classic competitive AR antagonists.

Here we report that BMS-986365 is a potent and selective degrader of AR^{WT} and of most of the clinically relevant LBD mutant forms of this receptor. BMS-986365 does not degrade ARV7, the most highly characterized AR splicing variant. While both VCaP and 22Rv1 express ARV7, BMS-986365 potently inhibits androgen-stimulated VCaP cell proliferation but does not inhibit the growth of 22RV1 cells *in vitro*. These data suggest that ARV7 positivity does not always predict resistance to BMS-986365. ARV7 has been shown to be associated with resistance to ENZ and abiraterone (48). However, the relative contribution of full-length AR versus ARVs to resistance remains to be determined since expression of ARV7 is often associated with upregulation of full-length AR (49).

EPI-7386, the most advanced clinical compound that targets ARVs, has not demonstrated meaningful clinical benefit (50).

CRBN-mediated AR degradation is a key driver of BMS-986365 pharmacology in mCRPC preclinical models. Importantly, however, BMS-986365 also displayed AR inhibitory activity when AR degradation was blocked, suggesting that BMS-986365 has substantial intrinsic antagonistic activity that likely contributes in a significant way to its therapeutic efficacy under conditions where residual AR exists. The intrinsic antagonism activity of BMS-986365 is a result of intentional medicinal chemistry design, balancing degradation potency and intrinsic agonism. Partial agonism is an issue for conventional AR inhibitors because it diminishes their antitumor activities, which is particularly notable in the context of AR overexpression (8). Our data suggest that agonism is also an issue for AR degraders as we have established a positive correlation between AR degradation potency and intrinsic agonism. We believe that this is due to a unique feature of AR compared with other nuclear hormone receptors, in that it requires an intramolecular interaction between the amino terminus and the carboxyl terminus to stabilize ligand binding (51). This interaction enables the presentation of protein–protein interaction surfaces that facilitate its transcriptional activity (52, 53). The challenge, therefore, was to identify ligands with sufficient affinity to allow efficient degradation of the receptor with minimal agonism. We accomplished this goal in an extensive SAR campaign that balanced degradation potency and intrinsic agonism, yielding BMS-986365.

Our preclinical data demonstrated that the dual functionality of BMS-986365 led to deeper and more potent blockade of AR signaling and better antitumor activity than with ENZ in multiple preclinical models of CSPC and mCRPC. Importantly, BMS-986365 displayed substantial efficacy in ARPI-resistant mCRPC xenograft models, an activity that appears to translate to humans, with early clinical testing of BMS-986365 in patients with ARPI-resistant mCRPC showing a 50% or greater

reduction in PSA in 50% of patients treated at the highest dose level. While clinical efficacy was still not observed in a significant proportion of patients, the presence of an AR mutation was not a requisite for responses, which were observed in both AR^{WT} and AR-mutant-expressing mCRPC cases (35). The limited clinical data generated from studies with other heterobifunctional molecules also support the likely utility of AR degraders in patients with ARPI-resistant mCRPC. However, in these studies, the therapeutic efficacy was, for the most part, limited to patients whose tumors expressed AR mutants (54). This raises the possibility that the expression of an AR mutation serves as a biomarker for AR-dependent disease and/or that among different AR degraders, there will be different clinical response profiles. Indeed, BMS-986365 has demonstrated clinical efficacy regardless of tumor AR mutational status, as exemplified herein (Fig. 6), with a durable clinical response noted in a patient with mCRPC harboring AR amplification without mutation (35, 55). These clinical findings align with our preclinical data and together support the conclusion that AR plays a key role in mCRPC that expresses WT or mutant AR in the post ARPI setting.

Lower intrinsic agonism intentionally engineered into BMS-986365 could be of particular relevance for the activity observed against tumors expressing AR^{WT}. The objective of using a degrader approach to eliminate AR expression in cells is to achieve absolute inhibition of androgen signaling. However, the degradation efficacy of AR degraders will likely be limited by homeostatic feedback systems that are hardwired into cells to enable them to maintain the receptor at a level required for viability. Important in this regard was the identification by Cai *et al.* (19) of a negative feedback loop in PC in which ligand-activated AR was shown to suppress the expression of AR mRNA. Thus, as the level of AR inhibition increases, so too does the activity of opposing events that increase AR expression. Indeed, in models lacking an AR mutation (VCAP, CTG-2441, and CTG-2440; Supplementary Fig. 5; Fig. 5), we observed dramatic upregulation of AR expression in

response to inhibition by ENZ or BMS-986365. In additional four models expressing mutant AR (LNCaP, 22Rv1, CWR22Pc-HR, and MDA-PCa-2b; Supplementary Fig. 5; Supplementary Table S15) the negative feedback mechanism on AR expression was less apparent. Thus, while AR mutations represent one way that PC cells can develop ARPI resistance, high-level AR^{WT} expression, further upregulated via feedback mechanisms, could represent an alternate and more common ARPI resistance mechanism. In the CTG-2440 model, for example, ENZ treatment resulted in the upregulation of AR expression, whereas BMS-986365 reduced AR protein levels. Nonetheless, ~60% of AR remained at the end of the efficacy study (Fig. 5C, bottom left), a residuum that could remain sensitive to activation by a binder with significant intrinsic agonism. Regardless of the underlying mechanisms, these preclinical observations, coupled with our reported clinical data, strongly support the potential for BMS-986365 to overcome ARPI-resistant disease regardless of AR mutational status. Collectively, these findings establish BMS-986365 as a first-in-class, dual AR degrader, and competitive antagonist that is likely to emerge as an important tool in the armamentarium used to treat patients with PC.

Authors' Contributions

S. Nayak: Conceptualization, data curation, formal analysis, supervision, validation, investigation, visualization, methodology, writing-review, and editing. **J.D. Norris**: Conceptualization, data curation, formal analysis, validation, investigation, visualization, methodology, writing-review, and editing. **M. Ammirante:** Conceptualization, data curation, formal analysis, methodology, writing-review, and editing. **E. Rychak:** Conceptualization, data curation, formal analysis, methodology, writing-review, and editing. **S.E. Wardell:** Conceptualization, data curation, formal analysis, validation, investigation, visualization, methodology, writing-review, and editing. **D. Liao:** Conceptualization, data curation, formal analysis, methodology, writing-review, and editing. **B. Toyama:** Conceptualization, data curation, formal analysis, methodology, writing-review, and editing. **R. Kandimalla:** Data curation, formal analysis, methodology, writing-review, and editing. **A. Christoforou:** Conceptualization, data curation, formal analysis, methodology, writing-review, and editing. **T. Tsuji:** Conceptualization, data curation, formal analysis, methodology, writing-review, and editing. **K. Liu:** Conceptualization, data curation, formal analysis, methodology, writing-review, and editing. **M. Tran:** Data curation, formal analysis, methodology, writing-review, and editing. **J. Meiring:** Data curation, formal analysis, methodology, writing-review, and editing. **S. Reiss:** Data curation, formal analysis, methodology, writing-review, and editing. **J.R. Piccotti:** Conceptualization, data curation, formal analysis, and supervision. **J.M. Baughman:** Conceptualization, data curation, formal analysis, methodology, writing-review, and editing. **C. Fontanillo:** Data curation, formal analysis, methodology, writing-review, and editing. **M. Khater:** Data curation, formal analysis, methodology, writing-review, and editing. **D.S. Mortensen:** Data curation, formal analysis, writing-review, and editing. **B. Cathers:** Conceptualization, supervision, validation, writing-review, and editing. **N. Bence:** Conceptualization, supervision, validation, writing-review, and editing. **D.W. Pierce:** Conceptualization, supervision,

validation, writing-review, and editing. **V. Plantevin-Krenitsky:** Conceptualization, data curation, formal analysis, supervision, validation, investigation, visualization, writing-review, and editing. **D. Rathkopf:** Data curation, writing-review, and editing. **J.D. Hansen:** Conceptualization, data curation, formal analysis, supervision, validation, investigation, visualization, writing-review, and editing. **L.G. Hamann:** Conceptualization, supervision, validation, writing-review, and editing. **R. Krishna Narla:** Conceptualization, data curation, formal analysis, supervision, validation, investigation, writing-review, and editing. **V.K. Arora:** Conceptualization, data curation, writing-original draft, writing-review, and editing. **D.P. McDonnell:** Conceptualization, formal analysis, supervision, validation, investigation, visualization, writing-original draft, writing-review, and editing. **M. Rolfe:** Conceptualization, supervision, validation, writing-review, and editing. **S. Xu:** Conceptualization, data curation, formal analysis, supervision, validation, investigation, visualization, writing-original draft, writing-review, and editing

Acknowledgments

The authors thank the entire BMS-986365 discovery and development teams including members from various functions for their project support and/or input to the manuscript preparation. Specifically, we thank Evan Horn, Marie Nguyen, Amber Wells, Jennifer Han, Jiaju Wu, Iryna Shnitsar, Mario Maira-Arce, Shailaja Kasibhatla, Ellen Filvaroff, Lisa Sapinoso, Nadia Guerrero, Catherine Fournier, Evan Holmes, Lin Tang, Deepak Dalvie, Yang Tang, April Bai, Julius Apuy, Lihong Shi, Laurie LeBrun, Jin Jen, Jason Haelewyn, Frans Baculi, Heather Venant, Courtney Havens, Uma Sundaram, Christopher Mayne, Brandon Whitefield, Dehua Huang, Jingjing Zhao, John Sapienza, Mark Nagy, Stephen Norris, Lida Tehrani, Roy Harris, Virginia Grant, Matthew Correa, Jean Francisco Brazeau, Kai Wang, Roberto Guzman, Kamran Ghoreishi, Xianshu Huang, Kung-I Feng, Jennifer G. Baker, Yeeun Bae, Si Han Chen, Nancy Delaet, Maria Stella deBiase, Kaleen

Barbary, and Tara Miller for their contribution to this project. We thank Ryan Kunz, Brian Erickson, and the IQ Proteomics team for advice and multiplexed proteomics assays. We would also like to thank Rupert Vessey, Gondi Kumar, and James Hartke for their leadership and strong support to this project. This work was supported by Bristol Myers Squibb. Professional medical writing and editorial assistance were provided by Benjamin Levine, Ph.D., and Tina Allen, BA, of Spark (a division of Prime, New York, USA), funded by Bristol Myers Squibb, according to Good Publication Practice guidelines.

REFERENCES

1. Siegel RL, Miller KD, Wagle NS, Jemal A. Cancer statistics, 2023. CA Cancer J Clin 2023;73:17–48.
2. Samson DJ, Seidenfeld J, Schmitt B, Hasselblad V, Albertsen PC, Bennett CL, et al. Systematic review and meta-analysis of monotherapy compared with combined androgen blockade for patients with advanced prostate carcinoma. Cancer 2002;95:361–76.
3. Watson PA, Arora VK, Sawyers CL. Emerging mechanisms of resistance to androgen receptor inhibitors in prostate cancer. Nat Rev Cancer 2015;15:701–11.
4. Robinson D, Van Allen EM, Wu YM, Schultz N, Lonigro RJ, Mosquera JM, et al. Integrative clinical genomics of advanced prostate cancer. Cell 2015;161:1215–28.
5. Chen CD, Welsbie DS, Tran C, Baek SH, Chen R, Vessella R, et al. Molecular determinants of resistance to antiandrogen therapy. Nat Med 2004;10:33–9.
6. Visakorpi T, Hyytinen E, Koivisto P, Tanner M, Keinänen R, Palmberg C, et al. In vivo amplification of the androgen receptor gene and progression of human prostate cancer. Nat Genet 1995;9:401–06.
7. Chang CY, Walther PJ, McDonnell DP. Glucocorticoids manifest androgenic activity in a cell line derived from a metastatic prostate cancer. Cancer Res 2001;61:8712–17.
8. Tran C, Ouk S, Clegg NJ, Chen Y, Watson PA, Arora V, et al. Development of a second-generation antiandrogen for treatment of advanced prostate cancer. Science 2009;324:787–90.
9. Beer TM, Tombal B. Enzalutamide in metastatic prostate cancer before chemotherapy. N Engl J Med 2014;371:1755–56.
10. Scher HI, Fizazi K, Saad F, Taplin ME, Sternberg CN, Miller K, et al. Increased survival with enzalutamide in prostate cancer after chemotherapy. N Engl J Med 2012;367:1187–97.
11. Ryan CJ, Smith MR, de Bono JS, Molina A, Logothetis CJ, de Souza P, et al. Abiraterone in metastatic prostate cancer without previous chemotherapy. N Engl J Med 2013;368:138–48.
12. de Bono JS, Logothetis CJ, Molina A, Fizazi K, North S, Chu L, et al. Abiraterone and increased survival in metastatic prostate cancer. N Engl J Med 2011;364:1995–2005.
13. Norris JD, Ellison SJ, Baker JG, Stagg DB, Wardell SE, Park S, et al. Androgen receptor antagonism drives cytochrome P450 17A1 inhibitor efficacy in prostate cancer. J Clin Invest 2017;127:2326–38.
14. Fizazi K, Tran N, Fein L, Matsubara N, Rodriguez-Antolin A, Alekseev BY, et al. Abiraterone acetate plus prednisone in patients with newly diagnosed high-risk metastatic castration-sensitive prostate cancer (LATITUDE): final overall survival analysis of a randomised, double-blind, phase 3 trial. Lancet Oncol 2019;20:686–700.
15. James ND, de Bono JS, Spears MR, Clarke NW, Mason MD, Dearnaley DP, et al. Abiraterone for prostate cancer not previously treated with hormone therapy. N Engl J Med 2017;377:338–51.
16. Davis ID, Martin AJ, Stockler MR, Begbie S, Chi KN, Chowdhury S, et al. Enzalutamide with standard first-line therapy in metastatic prostate cancer. N Engl J Med 2019;381:121–31.
17. Armstrong AJ, Azad AA, Iguchi T, Szmulewitz RZ, Petrylak DP, Holzbeierlein J, et al. Improved survival with enzalutamide in patients with metastatic hormone-sensitive prostate cancer. J Clin Oncol 2022;40:1616–22.
18. Sowalsky AG, Ye H, Bhasin M, Van Allen EM, Loda M, Lis RT, et al. Neoadjuvant-Intensive Androgen Deprivation Therapy Selects for Prostate Tumor Foci with Diverse Subclonal Oncogenic Alterations. Cancer Res 2018;78:4716–30.
19. Cai C, He HH, Chen S, Coleman I, Wang H, Fang Z, et al. Androgen receptor gene expression in prostate cancer is directly suppressed by the androgen receptor through recruitment of lysine-specific demethylase 1. Cancer Cell 2011;20:457–71.
20. Abida W, Cyrta J, Heller G, Prandi D, Armenia J, Coleman I, et al. Genomic correlates of clinical outcome in advanced prostate cancer. Proc Natl Acad Sci U S A 2019;116:11428–36.

21. Antonarakis ES, Armstrong AJ, Dehm SM, Luo J. Androgen receptor variant-driven prostate cancer: clinical implications and therapeutic targeting. Prostate Cancer Prostatic Dis 2016;19:231–41.
22. Fizazi K, Bernard-Tessier A, Roubaud G, Utriainen T, Barthélémy P, Fléchon A, et al. Targeted Inhibition of CYP11A1 in Castration-Resistant Prostate Cancer. NEJM Evid 2024;3:EVIDoa2300171.
23. Laccetti AL, Chatta GS, Iannotti N, Kyriakopoulos C, Villaluna K, Moigne RL, et al. Phase 1/2 study of EPI-7386 in combination with enzalutamide (enz) compared with enz alone in subjects with metastatic castration-resistant prostate cancer (mCRPC). J Clin Oncol 2023;41:179.
24. Ito T, Ando H, Suzuki T, Ogura T, Hotta K, Imamura Y, et al. Identification of a primary target of thalidomide teratogenicity. Science 2010;327:1345–50.
25. Chamberlain PP, Hamann LG. Development of targeted protein degradation therapeutics. Nat Chem Biol 2019;15:937–44.
26. Bondeson DP, Mares A, Smith IE, Ko E, Campos S, Miah AH, et al. Catalytic in vivo protein knockdown by small-molecule PROTACs. Nat Chem Biol 2015;11:611–17.
27. Zengerle M, Chan KH, Ciulli A. Selective Small Molecule Induced Degradation of the BET Bromodomain Protein BRD4. ACS Chem Biol 2015;10:1770–77.
28. Snyder LB, Neklesa TK, Chen X, Dong H, Ferraro C, Gordon DA, et al. Abstract 43: Discovery of ARV-110, a first in class androgen receptor degrading PROTAC for the treatment of men with metastatic castration resistant prostate cancer. Cancer Res 2021;81:43.
29. Snyder L, Lee SH, Neklesa TK, Chen X, Dong H, Ferraro C, et al. Abstract ND03: Discovery of ARV-766, an androgen receptor degrading PROTAC® for the treatment of men with metastatic castration resistant prostate cancer. Cancer Res 2023;83:ND03.
30. A study to assess the safety, pharmacokinetics, and anti-tumor activity of oral HP518 in patients with metastatic castration-resistant prostate cancer [Internet]; [cited September 2024]. Available from: https://clinicaltrials.gov/study/NCT05252364.
31. A study evaluating the safety, pharmacokinetics, and activity of RO7656594 in participants with advanced or metastatic prostate cancer [Internet]; [cited September 2024]. Available from: https://clinicaltrials.gov/study/NCT05800665.
32. A study of AC176 for the treatment of metastatic castration resistant prostate cancer [Internet]; [cited September 2024]. Available from: https://clinicaltrials.gov/study/NCT05241613.
33. National Center for Biotechnology Information. PubChem Patent Summary for US-11149007-B2. https://pubchem.ncbi.nlm.nih.gov/patent/US-11149007-B2. Accessed Jan. 16, 2025. [Internet]; [cited Available from:
34. National Center for Biotechnology Information. PubChem Patent Summary for WO-2022272053-A1, Cereblon binding compounds, compositions thereof, and methods of treatment therewith. https://pubchem.ncbi.nlm.nih.gov/patent/WO-2022272053-A1. Accessed Jan. 16, 2025. [Internet]; [cited Available from:
35. Rathkopf D, Patel MR, Choudhury AD, Rasco D, Lakhani N, Hawley JE, et al. Safety and clinical activity of BMS-986365 (CC-94676), a dual androgen receptor ligand-directed degrader and antagonist, in heavily pretreated patients with metastatic castration-resistant prostate cancer. Ann Oncol 2024. doi: 10.1016/j.annonc.2024.09.005.
36. Ozers MS, Marks BD, Gowda K, Kupcho KR, Ervin KM, De Rosier T, et al. The androgen receptor T877A mutant recruits LXXLL and FXXLF peptides differently than wild-type androgen receptor in a time-resolved fluorescence resonance energy transfer assay. Biochemistry 2007;46:683–95.
37. Urushibara M, Ishioka J, Hyochi N, Kihara K, Hara S, Singh P, et al. Effects of steroidal and non-steroidal antiandrogens on wild-type and mutant androgen receptors. Prostate 2007;67:799–807.
38. Joseph JD, Lu N, Qian J, Sensintaffar J, Shao G, Brigham D, et al. A clinically relevant androgen receptor mutation confers resistance to second-generation antiandrogens enzalutamide and ARN-509. Cancer Discov 2013;3:1020–29.

39. Matyskiela ME, Zhang W, Man HW, Muller G, Khambatta G, Baculi F, et al. A cereblon modulator (CC-220) with improved degradation of Ikaros and Aiolos. J Med Chem 2018;61:535–42.
40. Milhollen MA, Traore T, Adams-Duffy J, Thomas MP, Berger AJ, Dang L, et al. MLN4924, a NEDD8-activating enzyme inhibitor, is active in diffuse large B-cell lymphoma models: rationale for treatment of NF-κB–dependent lymphoma. Blood 2010;116:1515-23.
41. Li Y, Chan SC, Brand LJ, Hwang TH, Silverstein KA, Dehm SM. Androgen receptor splice variants mediate enzalutamide resistance in castration-resistant prostate cancer cell lines. Cancer Res 2013;73:483–9.
42. Safi R, Wardell SE, Watkinson P, Qin X, Lee M, Park S, et al. Androgen receptor monomers and dimers regulate opposing biological processes in prostate cancer cells. Nat Commun 2024;15:7675.
43. Raheem O, Kulidjian AA, Wu C, Jeong YB, Yamaguchi T, Smith KM, et al. A novel patient-derived intra-femoral xenograft model of bone metastatic prostate cancer that recapitulates mixed osteolytic and osteoblastic lesions. J Transl Med 2011;9:185.
44. Gebrael G, Fortuna GG, Sayegh N, Swami U, Agarwal N. Advances in the treatment of metastatic prostate cancer. Trends Cancer 2023;9:840–54.
45. Yehya A, Ghamlouche F, Zahwe A, Zeid Y, Wakimian K, Mukherji D, et al. Drug resistance in metastatic castration-resistant prostate cancer: an update on the status quo. Cancer Drug Resist 2022;5:667–90.
46. Antonarakis ES, Zhang N, Saha J, Nevalaita L, Shell SA, Garratt C, et al. Real-world assessment of AR-LBD mutations in metastatic castration-resistant prostate cancer. J Clin Oncol 2023;41:204.
47. Ledet EM, Lilly MB, Sonpavde G, Lin E, Nussenzveig RH, Barata PC, et al. Comprehensive Analysis of AR Alterations in Circulating Tumor DNA from Patients with Advanced Prostate Cancer. Oncologist 2020;25:327–33.
48. Armstrong AJ, Halabi S, Luo J, Nanus DM, Giannakakou P, Szmulewitz RZ, et al. Prospective multicenter validation of androgen receptor splice variant 7 and hormone therapy resistance in high-risk castration-resistant prostate cancer: the PROPHECY study. J Clin Oncol 2019;37:1120–9.
49. Sharp A, Coleman I, Yuan W, Sprenger C, Dolling D, Rodrigues DN, et al. Androgen receptor splice variant-7 expression emerges with castration resistance in prostate cancer. J Clin Invest 2019;129:192–208.
50. https://investors.essapharma.com/2024-10-31-ESSA-Pharma-Announces-Termination-of-Phase-2-Study-Evaluating-Masofaniten-Combined-with-Enzalutamide-in-Patients-with-Metastatic-Castration-Resistant-Prostate-Cancer. Accessed April 4, 2025. [Internet]; [cited Available from:
51. Askew EB, Minges JT, Hnat AT, Wilson EM. Structural features discriminate androgen receptor N/C terminal and coactivator interactions. Mol Cell Endocrinol 2012;348:403–10.
52. Chang CY, McDonnell DP. Evaluation of ligand-dependent changes in AR structure using peptide probes. Mol Endocrinol 2002;16:647–60.
53. Norris JD, Joseph JD, Sherk AB, Juzumiene D, Turnbull PS, Rafferty SW, et al. Differential presentation of protein interaction surfaces on the androgen receptor defines the pharmacological actions of bound ligands. Chem Biol 2009;16:452–60.
54. Gao X, Burris III HA, Vuky J, Dreicer R, Sartor AO, Sternberg CN, et al. Phase 1/2 study of ARV-110, an androgen receptor (AR) PROTAC degrader, in metastatic castration-resistant prostate cancer (mCRPC). J Clin Oncol 2022;40:Abstract 17.
55. Rathkopf D, Patel MR, Choudhury AD, Rasco D, Lakhani N. First-in-human phase 1 study of CC-94676, an androgen receptor ligand-directed degrader, in patients with metastatic castration-resistant prostate cancer. ASCO GU Cancers Symposium; 2024; San Francisco, CA & Online; 2024.

FIGURE LEGENDS

Figure 1. The intrinsic antagonism activity of BMS-986365 is a result of balancing potency and agonism. **A,** Illustration of relationship between degradation potency and intrinsic agonism based on data generated in VCaP cells with amplified AR^{WT} gene**.** (Created in BioRender. [Xu, S]. [https://app.biorender.com/illustrations/687fe3c88442617ff4df05a5]) **B**, Antagonism and **C** agonism, of AR LDDs were evaluated in a 7-day proliferation assay in the absence (agonism mode, **C**) and presence of 0.1 nM R1881 (antagonism mode, **B**) with or without CC-220 as indicated. VCaP cells were grown in medium containing 5% csFBS for 24 hours, followed by treatment with compound alone (agonism mode, **C**) or compound along with 0.1 nM R881 (antagonism mode, **B**) and grown for 7 days. Cell viability was then assessed using Cell Titer Glo assay. Percent of control was calculated as percentage of DMSO + CC-220 treated wells to determine maximum percent control in agonist mode. Percent of control was similarly calculated as percent of DMSO or CC-220 treated wells in the antagonist mode. The t_0 was estimated as signal in unstimulated cells and expressed as percentage of the R1881-stimulated cells. The percent control growth was calculated by subtracting t_0 from the percent of control and the data used for determination of GI_{50} using a 4-parameter logistics fit. csFBS, charcoal-stripped fetal bovine serum.

Figure 2. BMS-986365 is a high-affinity competitive AR binder that potently degrades the receptor. A, Structure of BMS-986365 and an illustration of its mechanism of action. BMS-986365 is a heterobifunctional molecule with an AR binding moiety in blue linked to a CRBN-binding moiety in red. The primary mechanism of action of BMS-986365 is to recruit AR for CRBN E3 ligase-dependent ubiquitination and proteasome-dependent degradation. In addition, the molecule was designed to be a potent competitive AR inhibitor. **B**, BMS-986365 degrades AR in a $CRL4^{CRBN}$ E3 ligase and proteasome-dependent manner. **B**, VCaP cells were treated with 0.1 μM or 1.0 μM BMS-986365 alone for 6 hours or in combination with a proteasome inhibitor (MG132), a neddylation inhibitor that inactivates cullin-RING E3 ligases (MLN4924), or CC-220, which tightly binds CRBN and prevents CRBN-mediated ubiquitination of AR. The lysates were then analyzed by Western blot using AR and tubulin antibodies. **C and D,** BMS-986365 rapidly degrades AR and blocks AR target gene protein expression in VCaP cells. **C**, AR degradation rate was measured in VCaP cells in starved media (RPMI without phenol red containing 5% csFBS) treated with 5, 50, 500, and 5000 nM of BMS-986365 along with 0.1 nM R1881. Cells were lysed at 15 and 30 minutes, and 1, 2, 4, 6, 16, and 24 hours following treatment, and AR levels were quantitated using an AR ELISA. **D**, VCaP cells were seeded at 50,000 per well in a 96-well plate in starved media (RPMI without phenol red containing 5% csFBS). After 24 hours, cells were treated with compounds at the indicated concentrations and 0.1 nM R1881 for 30 minutes, and 2, 4, 6, 24, 48, and 72 hours. Lysates were normalized by protein concentration and subjected to SDS PAGE and Western blotting using anti-AR, FKBP5, PSA, and β-actin antibodies. **E and F,** Determination of AR degradation rate by SILAC. VCaP (**E**) and LNCaP (**F**) cells were cultured in 48-well plates in SILAC light media for 48 and 96 hours, respectively. After washing the cells with PBS twice, the cells were incubated in SILAC medium media with indicated compounds and concentrations, and samples harvested at 0, 30 min, 1, 3, 6, 12, 24, and 48 hours. Samples were prepared and processed for targeted mass spectrometry as described in the Methods section. Plotted is the percent of the light form of the indicated peptide, normalized to the t=0 time point. The LOQ line represents the protein levels above which quantitation is within the linear assay range and can be performed with high confidence. Error bars represent +/- 1 standard deviation from three biological replicates. Basal AR protein levels were notably higher in VCaP than in LNCaP, resulting in less of the turnover curve being above LOQ in LNCaP. csFBS, charcoal-stripped fetal bovine serum; PBS, phosphate-buffered saline.

Figure 3. BMS-986365 exhibits superior AR inhibitory activity than ENZ in AR^{WT} setting via AR degradation and intrinsic antagonism via dual mechanism. A, BMS-986365 potently inhibits R1881-stimuated proliferation of VCaP and LNCaP cells but exhibits not anti-proliferative effect in 22Rv1 or PC3 cells. **B.** Inhibition of R1881-stimulated FKBP5 expression in VCaP cells by BMS-986365 in the presence or absence of CC-220. ENZ was used as a control. VCaP cells were evaluated in antagonist mode in the presence of 0.3 nM R1881 with the indicated compounds at concentrations ranging from 0.0005 to 10 μM for 24 hours (or in combination with 30 μM CC-220 as indicated). The level of FKBP5 expression was determined using a bDNA assay of cell lysates as a percent of control (0.3 nM R1881 alone). Percent of control values were used to calculate IC_{50} values for each compound/treatment condition using a 4-parameter logistic model or sigmoidal dose–response model (Fit Model 205). Each symbol represents mean percent of control of FKBP5 expression, with error bars depicting standard deviation of the mean of three independent experiments. bDNA, branched deoxyribonucleic acid. **C**, Inhibition of R1881-stimulated proliferation of VCaP cells by BMS-986365 in the presence or absence of CC-220. ENZ was used as a control. **D,** BMS-986365 causes deeper and faster inhibition of R1881-mediated AR function than ENZ. VCaP cells were treated with DMSO, 0.3 nM R1881 alone or 0.3 nM R1881 with compounds as indicated. A NanoString assay was used to evaluate a panel of 114 AR-regulated genes and 19 housekeeping genes. The

gene list and normalized data are included in Supplementary Table S10. The heatmaps display gene expression levels at different concentrations and time points were individually compared with gene-expression levels of the corresponding DMSO controls, and these derived gene expression log2 fold changes were plotted in the heatmaps. Experiments were performed in duplicate, and averaged data are shown. **E**, BMS-986365 reverses R1881-stimulated AR target gene expression with a potency similar to ENZ even when degradation is blocked by CC-220 cotreatment. VCaP cells were treated with DMSO, 0.3 nM R1881 alone, or 0.3 nM R1881 with 0.1, 1, or 10 μM of BMS-986365 or ENZ, with or without 30 μM CC-220 for 24 hours. A NanoString assay was used to evaluate a panel of 394 AR-regulated genes and 19 housekeeping genes. The heatmaps display gene expression levels at different treatment conditions compared with the corresponding DMSO controls. The derived log2 fold changes in gene expression were plotted in the heatmaps. Experiments were performed in triplicate and the average data were used for analysis.

Figure 4. BMS-986365 degrades AR *in vivo* and demonstrates antitumor activities in CDX and PDX models resistance to ARPIs. A and B, ****$P < 0.0001$. BMS-986365 degrades tumor AR and suppresses AR-dependent transcription in intact VCaP xenograft mouse model. Male NSG mice were inoculated with 5 ×10^6 VCaP tumor cells into the right flank in intact male NSG mice. Mice with VCaP tumors of approximately 400 mm^3 were administered BMS-986365 at 30 mg/kg QDx3 (n = 4/time point). Plasma samples were harvested at indicated times to determine BMS-986365. Tumors were collected at the indicated time points and processed to detect AR levels with Western blots (**A**). Numbers in the blue bars represent percentage AR degradation in BMS-986365-treated tumors compared with vehicle. Percent degradation was calculated relative to the vehicle control. Plasma and tumor exposure of BMS-986365 is represented in red and blue lines, respectively. Statistical analysis was performed using a one-way analysis of variance with Bonferroni's multiple comparisons test with all the study groups and the data shown are in comparison with vehicle control group. Results are presented as mean values with error bars representing standard error of the mean. **B,** The same VCaP tumors collected were also used for NanoString analysis. A 600-gene NanoString panel was used to evaluate the impact of BMS-986365 on AR target gene expression in VCaP tumor samples at 6 and 24 hours after compound treatment. Each dot represents one gene. Red and blue denote genes that are upregulated and downregulated by AR signaling, respectively. Green dots are 152 proliferation genes regulated by AR. Purple dots represent genes that are not regulated by AR. QD(x3), daily dosing (for 3 consecutive days). **C**, BMS-986365 degrades AR in epididymis in a dose-dependent manner in dog and cynomolgus monkey. Dog and monkey were orally administrated once daily with vehicle or BMS-986365 at indicated doses for 7 days. AR levels in epididymis approximately 24 hours after the last dose were measured via IHC staining using an AR antibody. IHC, immunohistochemistry. **D**, BMS-986365 inhibits tumor growth in intact VCaP xenograft model. Male nu/nu mice were inoculated with 1 × 10^6 VCaP tumor cells into the right flank. Mice were randomized into treatment groups (n = 4–7/group) at the time of treatment initiation. Test article treatment started on day 13 when the tumors were approximately 150 mm^3. Tumor inhibition, calculated as the percentage difference in average tumor volume between BMS-986365-treated mice and vehicle-treated control mice on day 21, is shown to the right of the dose–response curve for each treatment dose. Results are presented as mean values with error bars representing standard error of the mean. Statistical analysis was performed using a 2-way analysis of variance with Bonferroni's multiple comparisons test with all the study groups and the data shown are in comparison with the vehicle control group. **E,** BMS-986365 inhibits tumor growth in intact VCaP xenograft model with acquired resistance to ENZ. Male NSG mice were inoculated with 2 × 10^6 EnzR-VCaP tumor cells into the right flank. Mice were randomized into treatment groups (n = 10/group) at the time of treatment initiation. Test article treatment started on day 13 when the tumors were approximately 150 mm^3. Tumor inhibition, calculated as the percentage difference in average tumor volume between BMS-986365-treated mice and vehicle-treated control mice on day 21, is shown to the right of the dose–response curve for each treatment dose. Results are presented as mean values with error bars representing standard error of the mean. Statistical analysis was performed using a 2-way analysis of variance with Bonferroni's multiple comparisons test with all the study groups and the data shown are in comparison with vehicle control group.

Figure 5. BMS-986365 degrades AR, suppresses AR-dependent transcription, and overcomes resistance to ADT and ARPI in PDX models. * $P < 0.05$; ** $P < 0.01$; *** $P < 0.001$; ****$P < 0.0001$. **A,** A comparison of AR mRNA levels in a pair of PDX models (CTG-2440 vs. CTG-2441) isolated from the same mCRPC patient suggests that ABI treatment increases AR gene transcription. **Top**, Schematic depicts the origins of CTG-2441 and CTG-2440 PDX models. **Bottom**, AR mRNA levels (**left**) and inferred AR activity (**right**) based on AR target gene expression in CTG-2441 and CTG-2440. ABI, abiraterone. **B,** Both BMS-986365 and ENZ inhibit AR function, increase AR mRNA levels, and exhibit antitumor activity in CTG-2441 mCRPC PDX models derived from tumor samples progressed at ADT treatment. Protein levels (**top left**), AR mRNA (**top middle**), as well as AR activities (**top right**) were evaluated in CTG-2441 tumor xenograft after 7

consecutive days of once-daily treatment with vehicle, BMS-986365 (60 mpk), and ENZ (50 mpk). Tumor samples were harvested and processed at 24 hours post-final dose for protein and RNA-seq evaluation. **Bottom:** Antitumor activities of BMS-986365 and ENZ in CTG-2441 xenograft model. BMS-986365, or ENZ as indicated. mpk, mg/kg. **C**, BMS-986365 shows better antitumor activity than ENZ in the CTG-2440 PDX model from tumor samples progressed on ABI treatment. **Top**, AR mRNA (**middle**) and protein levels (**left**) as well as AR activities (**right**) were evaluated in CTG-2440 tumor xenograft after 7 consecutive days of once-daily treatment with vehicle, BMS-986365 (60 mpk), and ENZ (50 mpk). **Bottom**: AR protein levels measured at the end of efficacy study (l**eft**) and antitumor activities of BMS-986365 and ENZ in CTG-2441 xenograft model (**right**).

Figure 6. PSA and radiographic response to BMS-98365 in a patient with AR^{WT} amplified mCRPC who previously progressed on ENZ. Figure 7. PSA (A) and Radiographic Response (B) to 400 mg twice daily of BMS-98365 in a patient with mCRPC (harboring an AR amplified with no LBD mutation) who previously progressed on ENZ

Figure 1

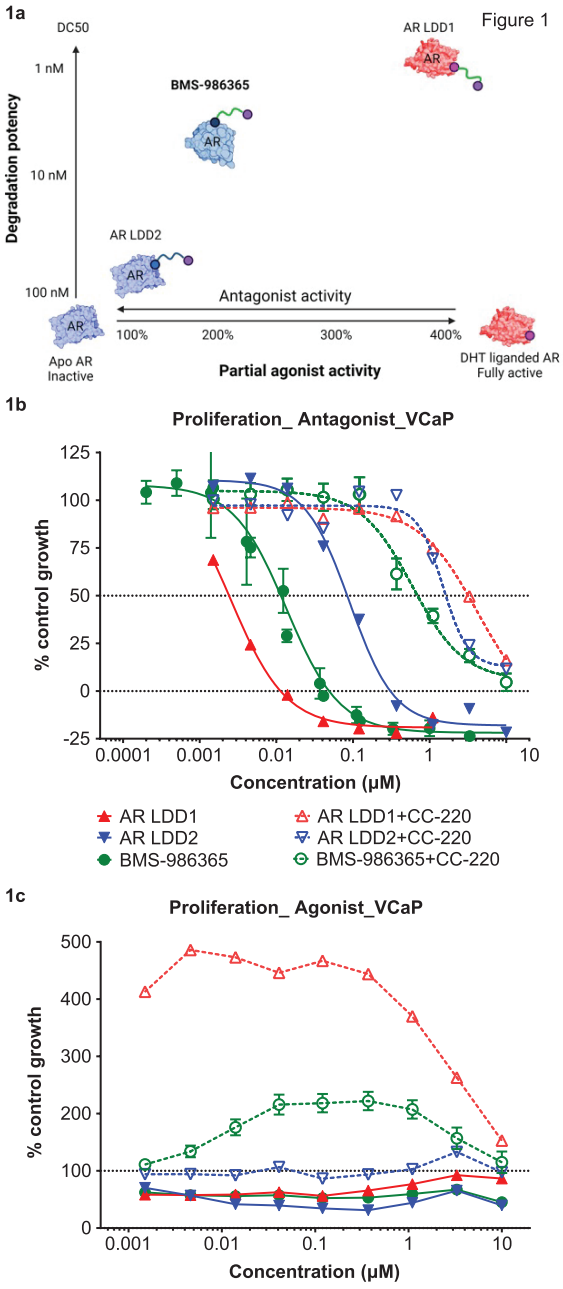

Figure 2

2a

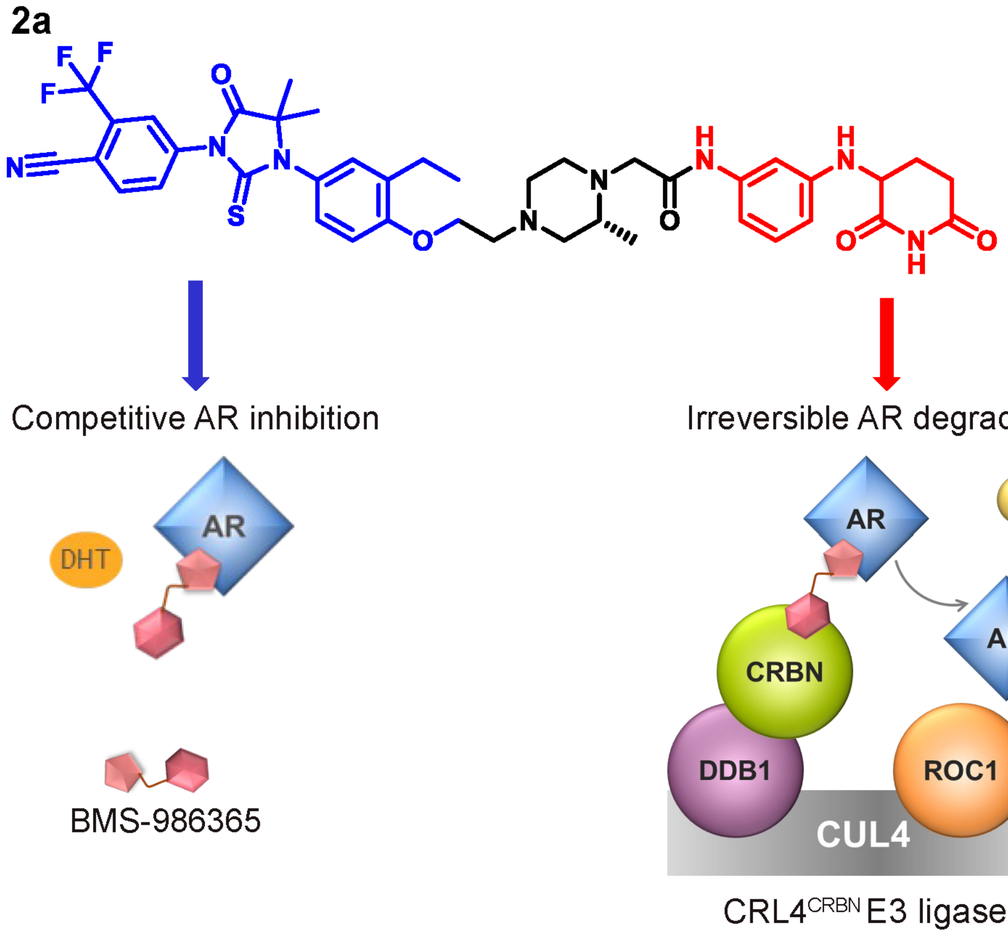

2b

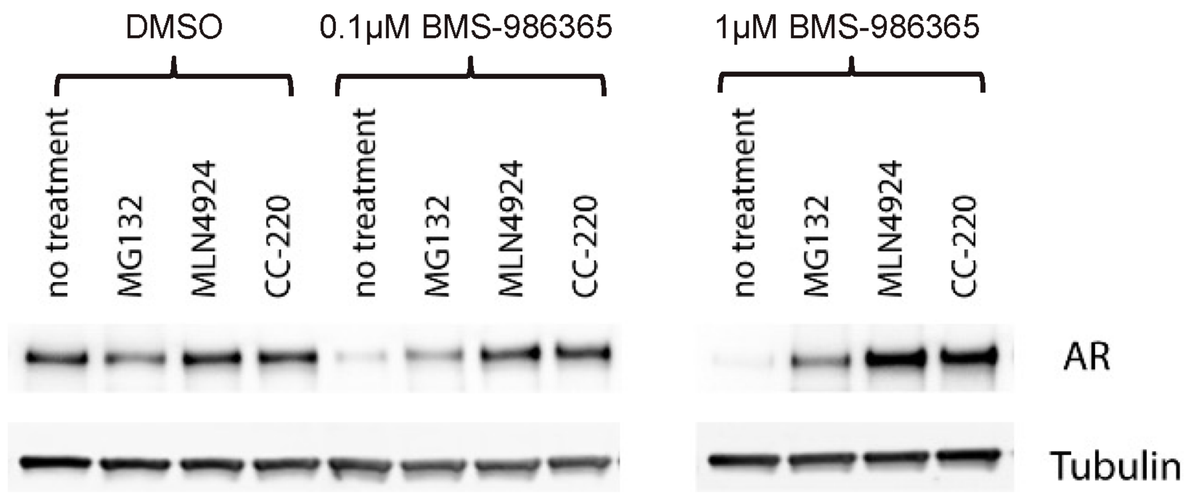

2c

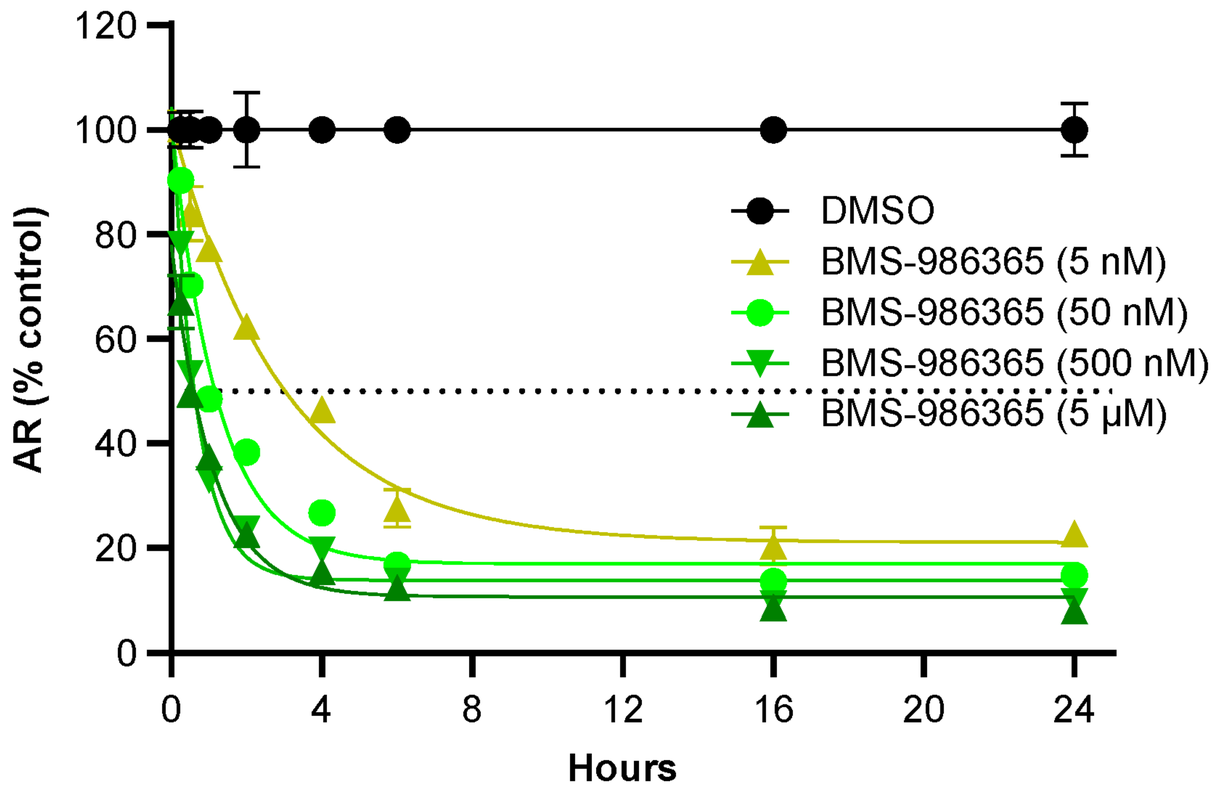

2d

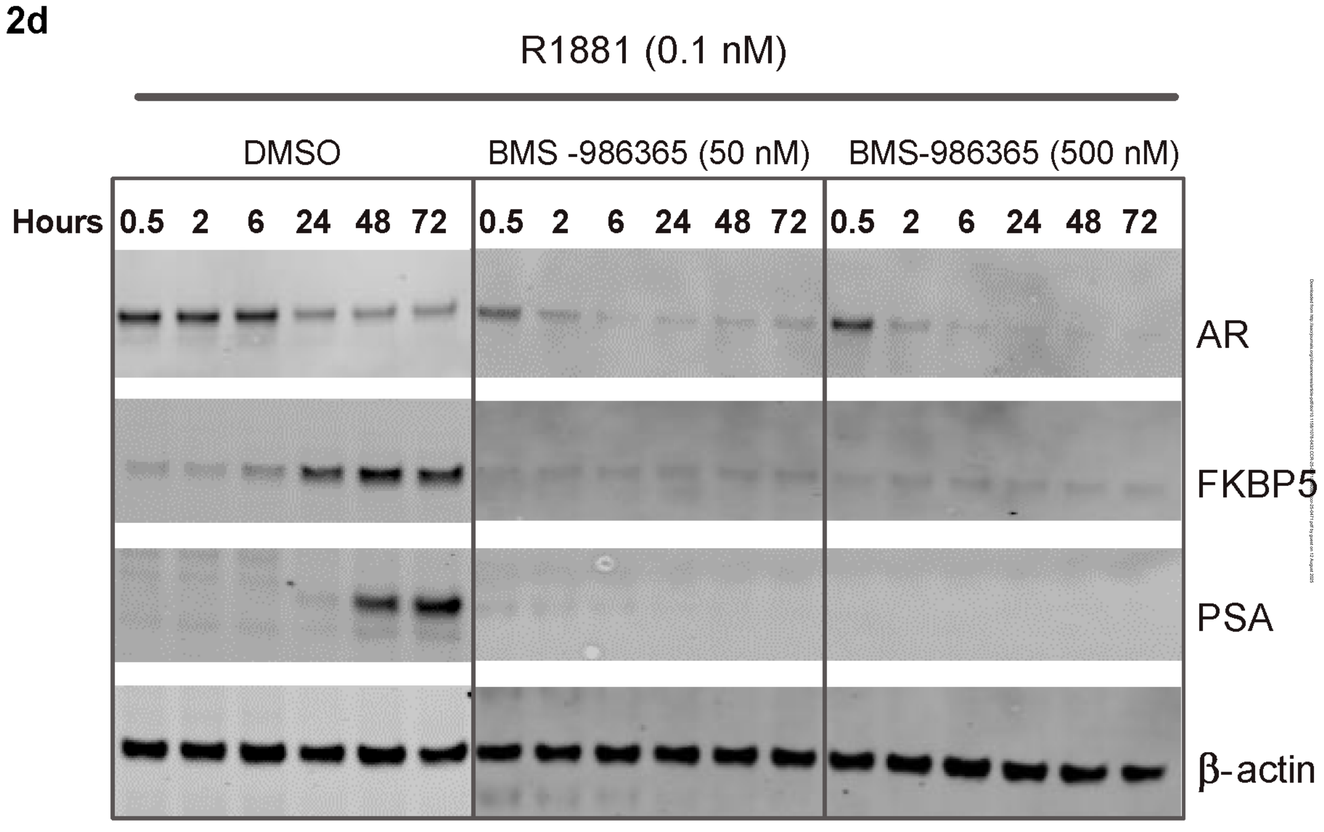

2e

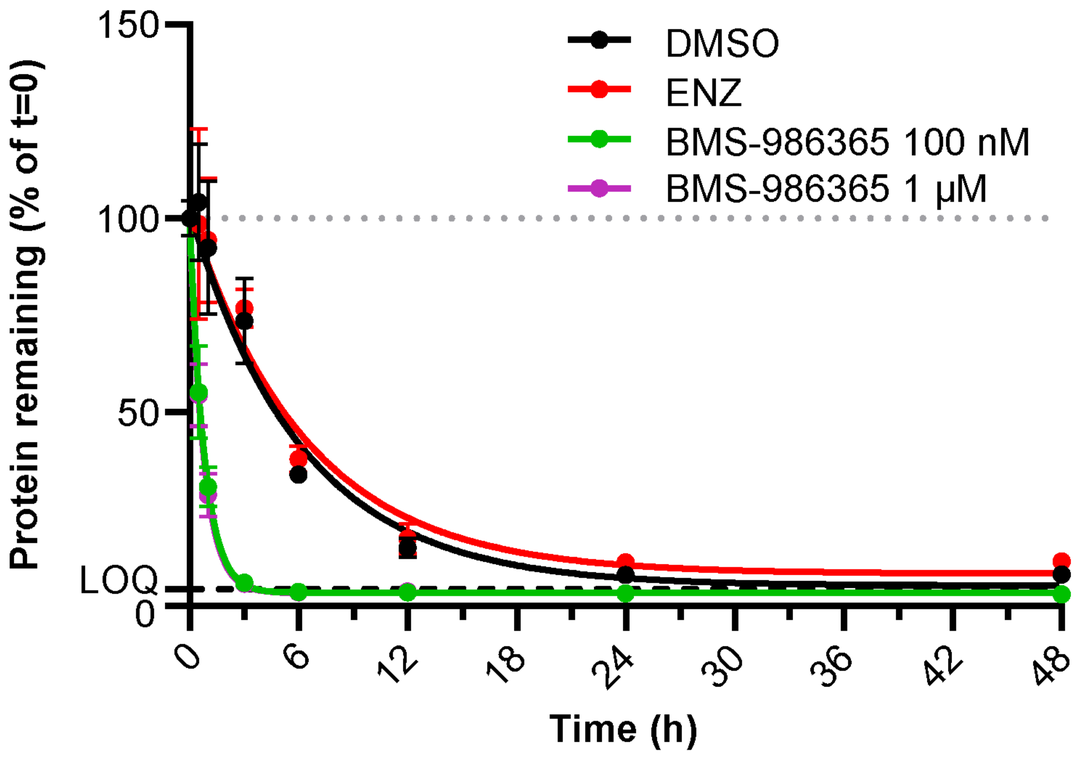

2f

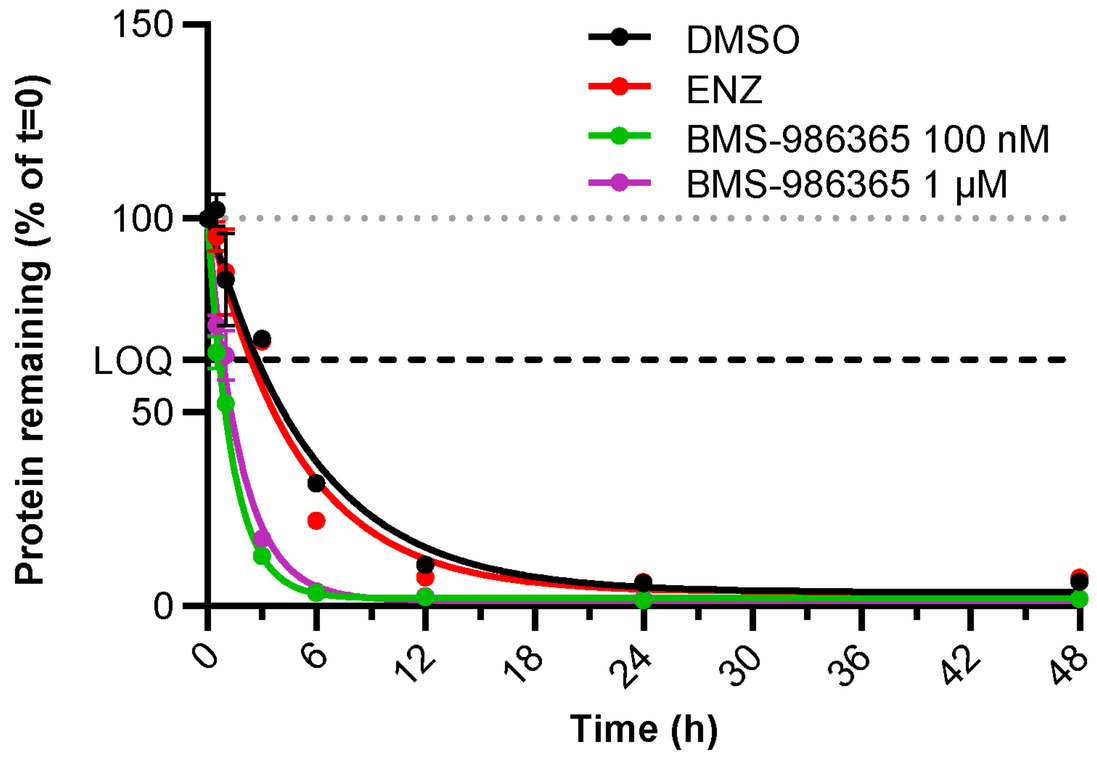

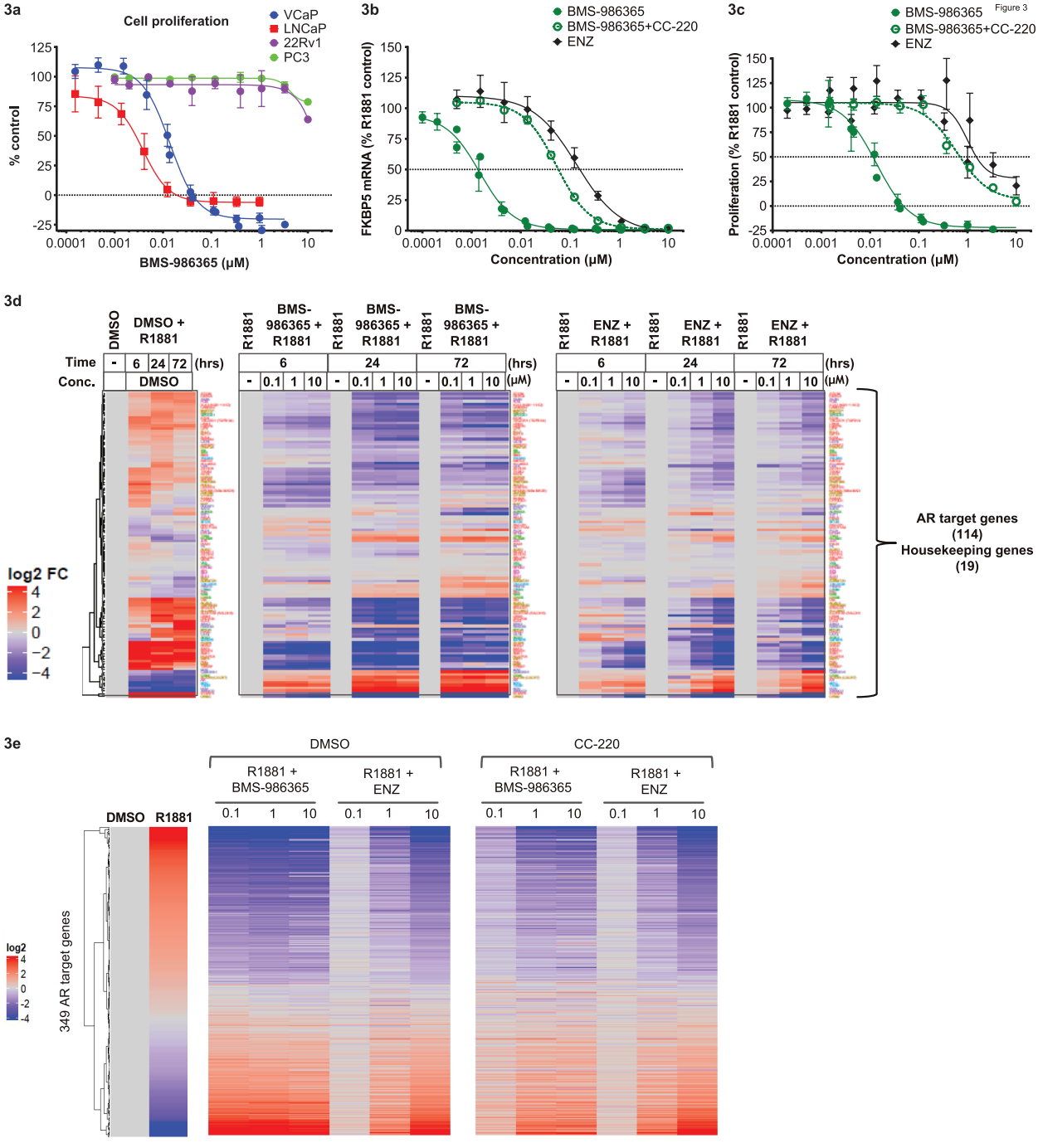

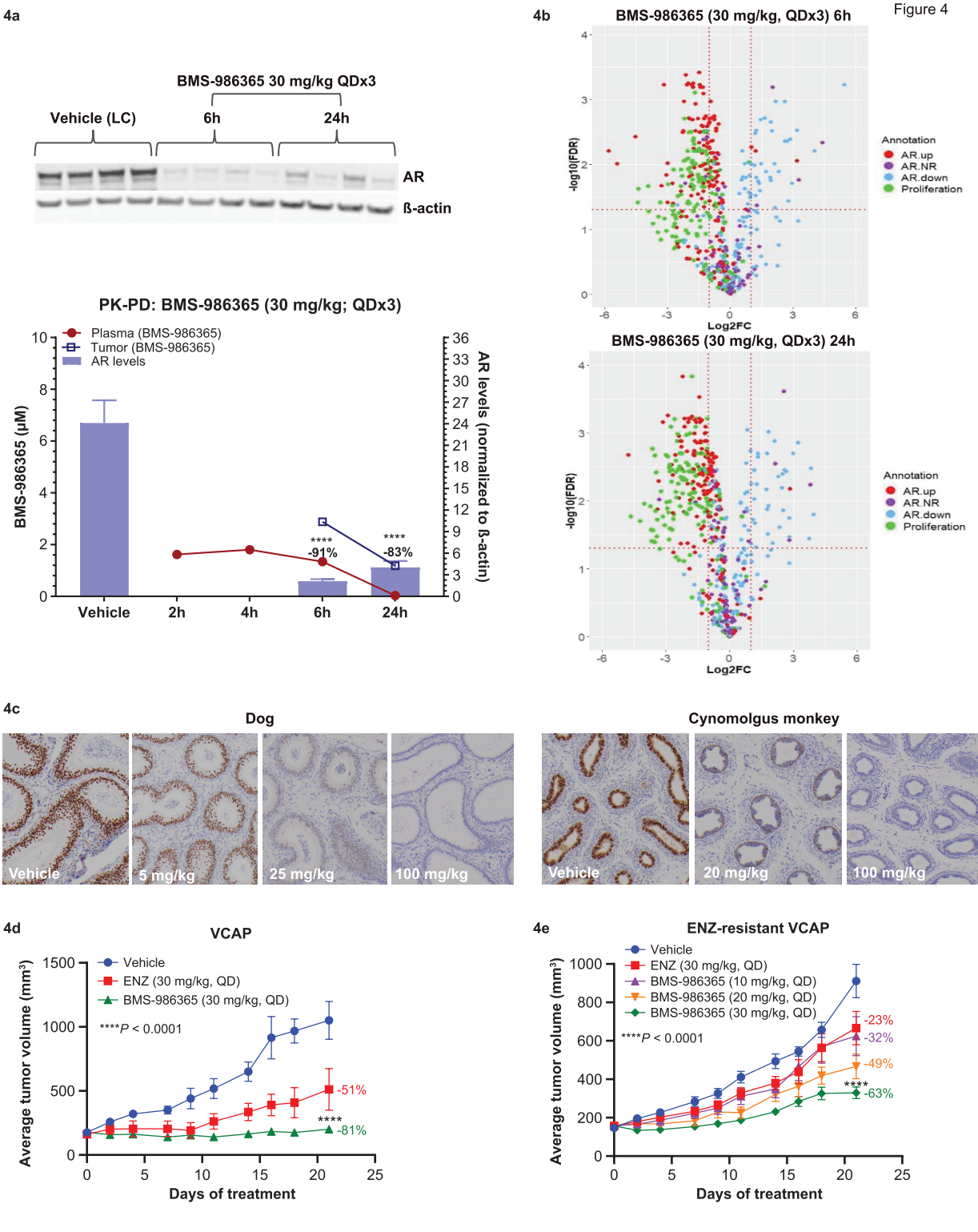

Figure 5

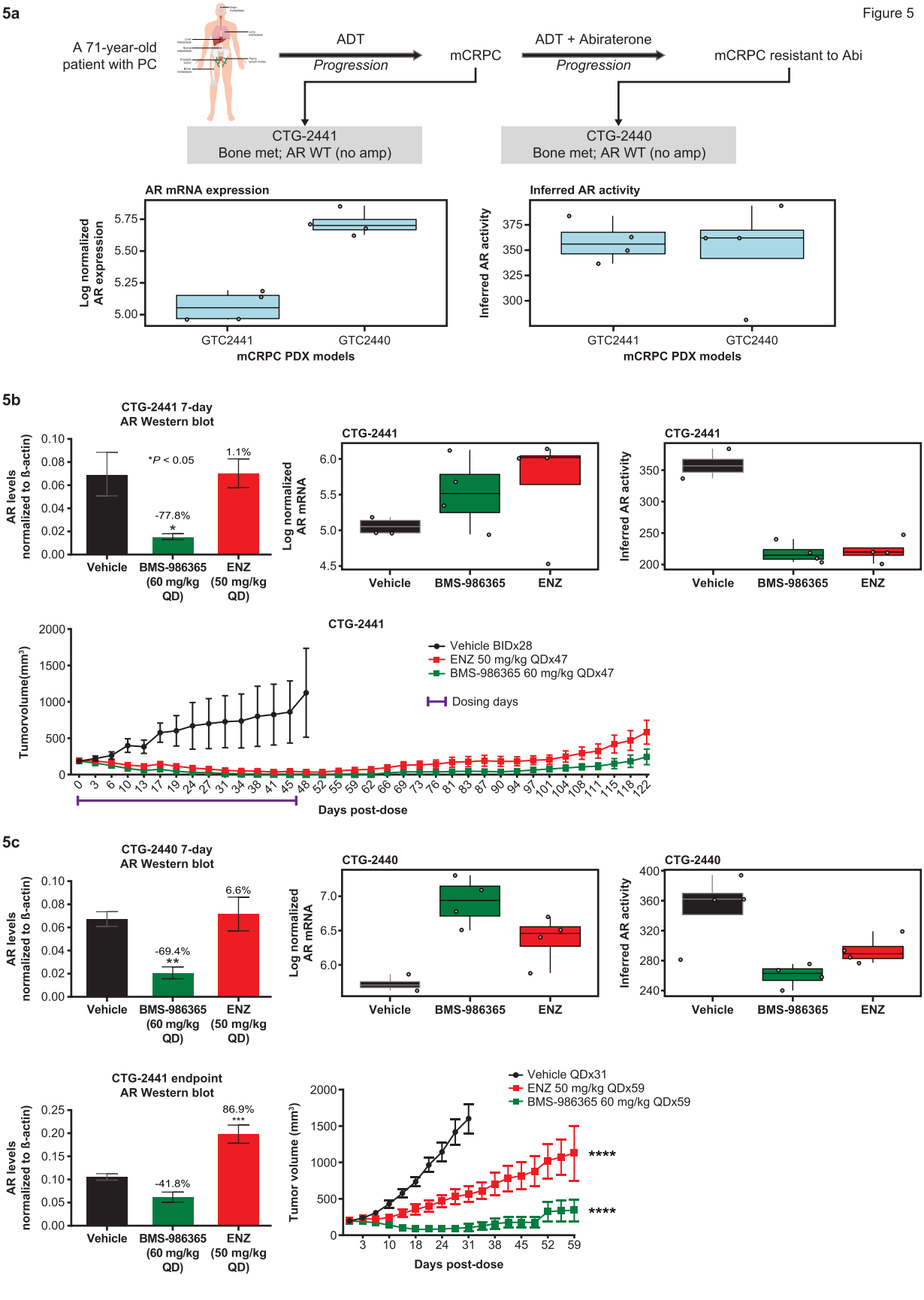

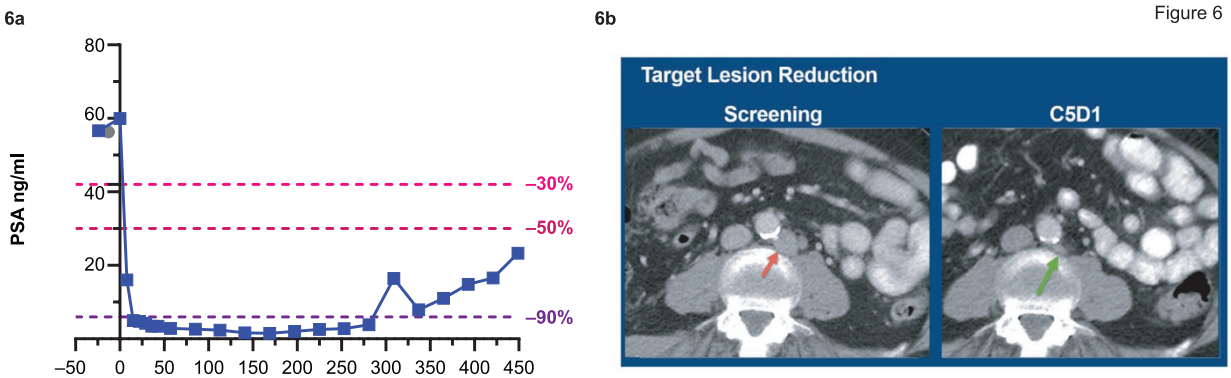

Figure 6